Coupled phengite ^{40}Ar–^{39}Ar geochronology and thermobarometry: *P-T-t* evolution of Andros Island (Cyclades, Greece)

BENJAMIN HUET*†, LOÏC LABROUSSE‡§, PATRICK MONIÉ¶,
BENJAMIN MALVOISIN‖ & LAURENT JOLIVET#**‡‡

*Department of Geodynamics and Sedimentology, University of Vienna, Althanstrasse 14, 1090 Vienna, Austria
‡UPMC Université Paris 06, UMR 7193, ISTeP, 4 place Jussieu, 75252 Paris cedex 05, France
§CNRS, UMR 7193, ISTeP, 4 place Jussieu, 75252 Paris cedex 05, France
¶Géosciences Montpellier, UMR 5573, Université Montpellier 2, France
‖Faculté des Géosciences et de l'Environnement, Université de Lausanne, Switzerland
#Université d'Orléans, ISTO, UMR 7327, 42071, Orléans, France
**CNRS/INSU, ISTO, UMR 7327, 42071, Orléans, France
‡‡BRGM, ISTO, UMR 7327, BP 36009, 45060 Orléans, France

Abstract – Andros is a key island for understanding both the timing of high-pressure–low-temperature (HP-LT) metamorphism and the dynamics of crustal-scale detachment systems exhuming high-grade units in the Cyclades (Greece). Using phengite ^{40}Ar–^{39}Ar geochronology coupled with thermobarometry, as well as data from literature, we constrain the pressure–temperature–time (*P-T-t*) paths of the Makrotantalon and Attic–Cycladic Blueschist units on Andros. Peak conditions of the HP-LT episode in the Makrotantalon unit are 550 °C and 18.5 kbar, dated at 116 Ma. We correlate this episode with Early Cretaceous blueschist facies metamorphism recognized in the Pelagonian zone of continental Greece. This is a new argument favouring a Pelagonian origin for the Makrotantalon unit. In the Attic–Cycladic Blueschist unit, the *P-T-t* path is characterized by: (1) exhumation after peak conditions in HP-LT conditions between 55 and 35 Ma; (2) isobaric heating at 7 kbar until 30 Ma; and (3) isothermal decompression until 21 Ma. This thermal evolution and timing are similar to those of the neighbouring Tinos Island, emphasizing major thermal re-equilibration at the transition between stable and retreating subduction. Modifications of the crustal thermal state played a major role in the evolution of the North Cycladic Detachment System, below which Andros HP-LT units were exhumed.

Keywords: *P-T-t* path, blueschist, HP-LT metamorphism, Aegean, detachments, subduction.

1. Introduction

High-pressure–low-temperature (HP-LT) metamorphic rocks witness ancient subduction or collision zones (Evans & Brown, 1986). Pressure–temperature–time (*P-T-t*) paths of such rocks provide major constraints on the evolution of orogens and the dynamics of exhumation processes active in these zones (Thompson & England, 1984; Ernst, 1988, 2001). However, linking time to *P-T* conditions requires that geochronology be tightly coupled with thermobarometry through petrology and mineral chemistry (Müller, 2003; Villa & Williams, 2012; Warren, Hanke & Kelley, 2012).

The Attic–Cycladic region in the Aegean (Greece) is one of the most studied HP-LT belts of the Mediterranean convergence domain. The tectono-metamorphic record in this part of the Hellenides indicates Eocene burial and exhumation in HP-LT conditions followed by Oligo-Miocene exhumation in low-pressure–high-temperature (LP-HT) conditions below crustal-

scale brittle–ductile detachment systems (Jolivet & Brun, 2010; Ring *et al.* 2010; Grasemann *et al.* 2012; Philippon, Brun & Gueydan, 2012). Within that time framework, two points are still poorly constrained. On the one hand, the meaning of Cretaceous ages determined in HP-LT rocks is debated (Bröcker & Enders, 1999, 2001; Tomaschek *et al.* 2003; Bröcker & Franz, 2006; Bulle *et al.* 2010; Huyskens & Bröcker, 2014). This point is important to correlate the tectonic events in the internal Hellenides with those of the Rhodope on the opposite side of the Vardar suture zone (Burg, 2012). On the other hand, precise time constraints on the activity of the different detachments systems and their individual segments are still missing. Deciphering *P-T-t* records in order to distinguish exhumation below detachment systems from earlier phases is a key issue in the understanding of the mechanical behaviour of detachment zones.

In this respect, Andros is a key island of the Attic–Cycladic region as part of the North Cycladic Detachment System, of which the timing and geometry are complex (Brichau *et al.* 2007, 2008; Jolivet *et al.* 2010). Besides, the significance of Early Cretaceous

†Author for correspondence: benjamin.huet@univie.ac.at

ages determined there remains unclear (Bröcker & Franz, 2006; Huyskens & Bröcker, 2014). Here we present results of ^{40}Ar–^{39}Ar geochronology coupled with thermobarometry from Andros island. Using also data from the literature, we constrain the local *P-T-t* record and discuss the implications on the evolution of the Hellenic subduction zone and the behaviour of detachments during exhumation of the HP-LT rocks in the Aegean.

2. Geological settings

2.a. Geology of the Cyclades

The Cycladic archipelago belongs to the Hellenides–Taurides belt that resulted from convergence between Africa and Eurasia in the Eastern Mediterranean during Mesozoic–Cenozoic time (Jacobshagen *et al.* 1978). It is now located in the Aegean Sea (Fig. 1a), the back-arc of the active Hellenic subduction zone (Le Pichon & Angelier, 1981). Three main palaeogeographical units are distinguished in the Cyclades (Fig. 1a; Bonneau, 1984): a basal unit correlated with the Gavrovo–Tripolitza nappe of the external zones (Avigad *et al.* 1997; Jolivet *et al.* 2004; Ring *et al.* 2007*a*, *b*); the middle Attic–Cycladic units (the Attic–Cycladic Blueschist unit and the Cycladic Basement); and the uppermost Pelagonian unit (Upper Cycladic Nappe).

The Attic–Cycladic units comprise a Permo-Mesozoic continental margin and remnants of an oceanic domain, the Attic–Cycladic Blueschist unit that is correlated with the Pindos Nappe, detached from its pre-alpine basement, the Cycladic Basement (Huet, Labrousse & Jolivet, 2009). They were affected by two metamorphic events (Altherr *et al.* 1979, 1982; Wijbrans & McDougall, 1986, 1988; Bröcker *et al.* 1993; Putlitz, Cosca & Schumacher, 2005; Lagos *et al.* 2007; Grasemann *et al.* 2012): a blueschist and eclogite facies episode during Eocene time (55–35 Ma) followed by retrogression in the greenschist and amphibolite facies during Oligo-Miocene time (30–15 Ma).

The Pelagonian unit consists of ophiolitic material obducted over a pre-alpine continental basement and its Palaeo-Mesozoic cover. In the Cyclades, it is characterized by LP-HT metamorphism yielding Late Cretaceous ages (Patzak, Okrusch & Kreuzer, 1994). Miocene greenschist-facies metamorphism locally affected the Pelagonian unit (Bröcker & Franz, 1998; Zeffren *et al.* 2005). Although Early and Late Cretaceous blueschists occur in the Pelagonian unit of Evia Island (Maluski *et al.* 1981), Olympos (Schermer, Lux & Burchfiel, 1990) and Ossa regions (Lips, White & Wijbrans, 1998), no high-pressure rock has yet been recognized in the Pelagonian unit from the Cyclades realm.

The contact separating the Attic–Cycladic units and the Pelagonian unit played a major role in the history of the Cyclades. As the boundary between the upper and lower plates of the Hellenic subduction zone, it acted during Eocene time as a thrust and then as a normal fault, leading successively to burial and syn-orogenic exhumation of the Attic–Cycladic units (Trotet, Jolivet & Vidal, 2001). After the Hellenic slab began to retreat 30–35 Ma ago (Jolivet & Faccenna, 2000), the Aegean lithosphere started to stretch, the HP-LT rocks then re-equilibrated in LP-HT conditions and were exhumed below several sets of detachments that partly reactivated the Pelagonian unit basal contact. Correlations between detachments lead to the identification of three major detachment systems (Fig. 1a): the North Cycladic Detachment System (NCDS, Jolivet *et al.* 2010); the Western Cycladic Detachment System (WCDS, Grasemann *et al.* 2012); and the Naxos–Paros Detachment System (NPDS, Gautier, Brun & Jolivet, 1993). When exposed, the Pelagonian unit systematically appears as the upper unit of all these detachments.

2.b. Geology of Andros

Three units are distinguished on Andros Island: the Attic–Cycladic Blueschist unit; the Makrotantalon unit; and an upper unit (Papanikolaou, 1978; Mehl *et al.* 2007). The Attic–Cycladic Blueschist unit is a metasedimentary sequence (schist, marble and interlayered metavolcanite) that contains bodies of ultramafic and metamorphosed basic and felsic magmatic rocks. U–Pb ages on detrital and magmatic zircons constrain the deposition age of the sedimentary sequence to Triassic–Jurassic time (Bröcker & Pidgeon, 2007; unpublished data cited in Huyskens & Bröcker, 2014). HP-LT rocks preserved from retrogression are mostly found along the SW coast (Papanikolaou, 1978; Mehl *et al.* 2007). They formed at 450–500 °C and a minimum pressure of 10 kbar (Reinecke, 1986) and were first exhumed in the glaucophane stability field in constrictive NE–SW stretching (Ziv *et al.* 2010). The Rb–Sr phengite ages in the range 40–50 Ma are considered to date this episode (Bröcker & Franz, 2006; Huyskens & Bröcker, 2014). Widespread retrogression in the greenschist facies is associated with brittle–ductile NE–SW stretching and top-to-the-NE shear (Mehl *et al.* 2007). Greenschist facies overprint occurred at conditions in the range 350–520 °C and 5–9 kbar (Bröcker & Franz, 2006) and is dated at 21–24 Ma by Rb–Sr phengite ages (Bröcker & Franz, 2006; Huyskens & Bröcker, 2014).

The upper unit, correlated with the Pelagonian unit, comprises intensely foliated greenschists and serpentinites lying over a breccia. It is separated from the Attic–Cycladic Blueschist unit by a detachment (Mehl *et al.* 2007) that is part of the NCDS (Jolivet *et al.* 2010). Rocks close to the contact yielded Rb–Sr phengite ages between 24 and 28 Ma (Huyskens & Bröcker, 2014). This is considered to date the activity of the NCDS on Andros.

The Makrotantalon unit is a metasedimentary sequence with characteristics distinct from the Attic–Cycladic Blueschist unit. It contains dolomitic marbles that yielded Permian fossils (Papanikolaou, 1978). U–Pb ages on detrital zircons are older than in the Attic–Cycladic Blueschist unit (*c.* 260 Ma,
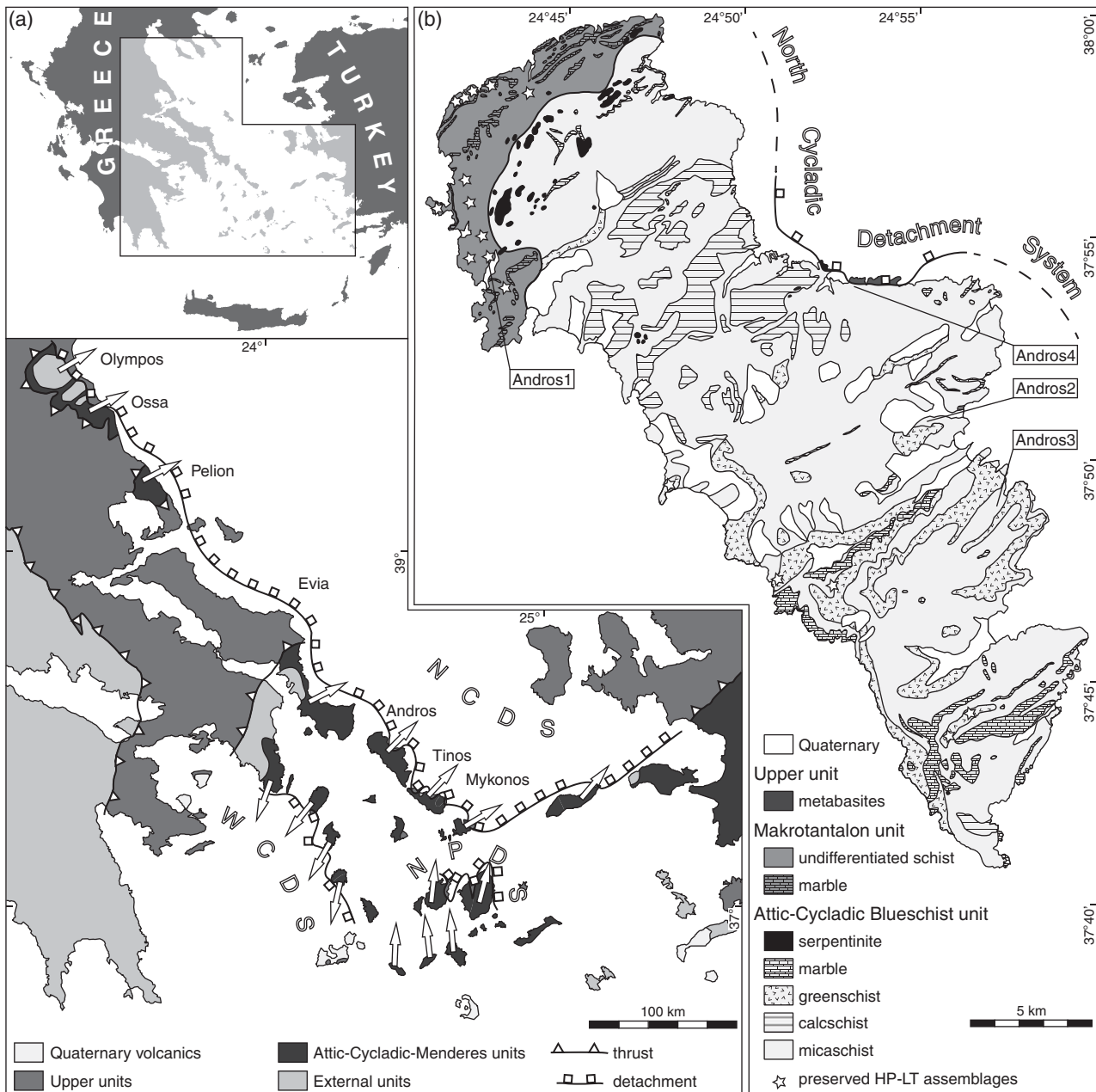
Figure 1. (a) Simplified geological map of the central Aegean, modified after Grasemann *et al.* (2012) and Jolivet *et al.* (2012). The Attic–Cycladic–Menderes unit regroups the Attic–Cylcadic Blueschist unit, the Cycladic basement, the Menderes basement and the Menderes cover. It appears as windows below the upper units: the Pelagonian unit (Olympos, Pelion, Ossa and Cyclades in Greece) and the Bornova flysch and Lycian nappes (Menderes massif in Turkey). It lies over the external units of the Hellenides. The Attic–Cycladic–Menderes unit has been exhumed below sets of low-angle normal faults: the North Cycladic Detachment system (NCDS), the West Cycladic Detachment System (WCDS) and the Naxos-Paros Detachment system (NPDS). The arrows indicate the sense of shear associated with these detachments. (b) Geological map of Andros island, after Mehl *et al.* (2007). The contact between the upper unit and the Cycladic Blueschist is a low-angle normal fault belonging to the NCDS (Jolivet *et al.* 2010). The contact between the Makrotantalon unit and the Cycladic Blueschist is not well defined everywhere (Huyskens & Bröcker, 2014) and follows serpentinite bodies (Papanikolaou, 1978). The stars indicate preserved HP-LT index minerals (Mehl *et al.* 2007; Huyskens & Bröcker, 2014). The investigated samples are also localized on the map.

unpublished data cited in Huyskens & Bröcker, 2014). Phengite Rb–Sr ages clustering around 80 Ma indicate a Late Cretaceous metamorphic event (Bröcker & Franz, 2006; Huyskens & Bröcker, 2014). Older ages (*c.* 105 Ma) have also been found. Index minerals for the HP-LT metamorphism described in mafic rocks (Mehl *et al.* 2007; Huyskens & Bröcker, 2014) show that HP-LT rocks are more widespread in the Mak-rotantalon unit than in the Attic–Cycladic Blueschist unit (Fig. 1b). However, the Makrotantalon and Attic–Cycladic Blueschist units have apparently shared the same LP-HT history. Greenschist facies deformation is continuous across the contact between the two units (Mehl *et al.* 2007). Similar Rb–Sr phengite ages and *P-T* conditions have been found in greenschist facies rocks of both (Bröcker & Franz, 2006; Huyskens &

Table 1. Samples location

Sample	Unit	Rock type	GPS coordinate	*P-T* conditions	Phengite $^{40}Ar/^{39}Ar$ radiochronology
Andros1	Makrotantalon	Garnet-glaucophane schist	37° 54.4′, 024° 42.5′	Phase diagram, Theriak-Domino	3 singles grains
Andros2	Attic–Cycladic Blueschist	Micaschist	37° 51.0′, 024° 55.6′	Phg-Chl multi-equilibrium, TWEEQU	2 single grains, 1 concentrate
Andros3	Attic–Cycladic Blueschist	Micaschist	37° 54.0′, 024° 53.2′	Phg-Chl multi-equilibrium, TWEEQU	–
Andros4	Attic–Cycladic Blueschist	Micaschist	37° 49.1′, 024° 57.4′	Phg-Chl multi-equilibrium, TWEEQU	–

Table 2. Representative electron microprobe analyses of garnet, glaucophane, phengite and chlorite from Makrotantalon and lower units

Mineral sample	Grt Andros1	Phg Andros1	Phg Andros1	Gln Andros1	Phg Andros2	Chl Andros2	Phg Andros3	Chl Andros3	Phg Andros4	Chl Andros4
SiO_2	37.98	49.66	48.92	57.28	49.52	27.11	50.06	25.08	49.05	25.59
TiO_2	0.09	n.a.	n.a.	0.07	n.a.	0.00	0.14	0.14	0.05	0.04
Al_2O_3	21.30	27.28	32.75	11.87	29.48	21.32	27.10	22.56	32.15	22.14
FeO	29.44	2.69	1.43	14.90	2.31	17.72	2.87	25.33	2.51	28.09
MnO	0.73	0.00	0.04	0.17	0.02	0.37	0.02	0.12	0.00	0.56
MgO	2.32	2.63	1.90	6.60	2.72	20.31	2.98	13.57	1.66	12.09
CaO	8.28	0.00	0.05	0.12	0.03	0.07	0.00	0.16	0.04	0.02
Na_2O	0.00	0.35	1.57	7.30	0.42	0.00	0.24	0.09	0.33	0.00
K_2O	0.00	10.57	9.09	0.01	10.51	0.00	10.00	0.03	9.72	0.02
Total	100.14	93.18	95.75	98.32	95.01	86.90	93.41	87.08	95.51	88.55
Si	3.00	3.40	3.22	7.96	3.32	2.76	3.41	2.66	3.25	2.71
Ti	0.00	–	–	0.01	–	0.00	0.01	0.01	0.00	0.00
Al	1.99	2.20	2.54	1.94	2.33	2.56	2.17	2.82	2.51	2.76
Fe^{3+}	0.01	–	–	0.05	–	–	–	–	–	–
Fe^{2+}	1.98	0.15	0.08	1.68	0.13	1.51	0.16	2.25	0.14	2.48
Mn	0.05	0.00	0.00	0.02	0.00	0.03	0.00	0.01	0.00	0.05
Mg	0.30	0.27	0.19	1.37	0.27	3.09	0.30	2.15	0.16	1.91
Ca	0.66	0.00	0.00	0.02	0.00	0.01	0.00	0.02	0.00	0.00
Na	0.00	0.05	0.20	1.97	0.05	0.00	0.03	0.02	0.04	0.00
K	0.00	0.92	0.76	0.02	0.90	0.00	0.87	0.00	0.82	0.00
Sum	7.99	6.99	6.99	15.04	7.00	9.96	6.95	9.94	6.92	9.91

n.a. not analysed; Fe^{3+} is not recalculated for phyllosilicates

Bröcker, 2014). Finally, the contact between the Makrotantalon unit and the Attic–Cycladic Blueschist unit is loosely defined by a series of serpentinite bodies (Papanikolaou, 1978) and its nature has been debated (see Bröcker & Franz, 2006; Mehl *et al.* 2007; Huyskens & Bröcker, 2014). According to the most recent interpretation, the contact was a thrust which was active at 40–45 Ma as constrained by Rb–Sr phengite ages (Huyskens & Bröcker, 2014).

3. Coupling thermobarometry and geochronology

Four representative samples selected from a collection of over 40 samples have been investigated (Fig. 1b, Table 1). Andros1 is a garnet-glaucophane schist from Makrotantalon unit. Andros2, Andros3 and Andros4 are micaschists sampled at different structural levels of the lower unit. Pressure–temperature conditions were estimated for all samples and phengite ^{40}Ar–^{39}Ar geochronology was performed on samples Andros1 and Andros2.

We used an electron microprobe to analyse the minerals belonging to the metamorphic assemblages in thin-sections (service Camparis, Université Pierre et Marie Curie-Paris 6, France; see Yamato *et al.* 2007). Representative electron microprobe analyses are presented in Table 2. Thermodynamic modelling of metamorphic assemblages and mineral compositions was carried out using Theriak-Domino software (de Capitani & Petrakakis, 2010) using the updated database of Holland & Powell (1998) available on the Theriak-Domino website (http://titan.minpet.unibas.ch/minpet/theriak/prog120103/). We used a chemical composition calculated with modal counting and microprobe analyses in order to avoid secondary and retrograde phases (Meyre *et al.* 1999). In the micaschists, the equilibrium conditions of phengite-chlorite pairs were calculated with TWEEQU (thermobarometry with estimation of equilibration state) multi-equilibrium thermobarometry (Berman, 1991; Vidal & Parra, 2000), according to the method described in Yamato *et al.* (2007). This method was successful for determining the *P-T* path of the neighbouring island of Tinos (Fig. 1a; Parra, Vidal & Jolivet, 2002).

^{40}Ar–^{39}Ar geochronology was performed at Géosciences Montpellier (Université Montpellier 2, France). Two different dating techniques were used. Five single

Table 3. ^{40}Ar/^{39}Ar phengite isotopic data for the dated single grains from Makrotantalon and lower units

Step no.	^{40}Ar/^{39}Ar	^{38}Ar/^{39}Ar	^{37}Ar/^{39}Ar	^{36}Ar/^{39}Ar $\times 10^{-3}$	%^{39}Ar released	%^{40}Ar*	^{40}Ar*/^{39}Ar$_K$	Age (Ma)	$\pm 1\sigma$ (Ma)
Andros1, J = 0.009901									
1	7.308	0.011	0.02666	4.312	5.50	82.38	6.02	104.46	3.83
2	6.930	0.009	0.12859	0.000	7.70	99.77	6.92	119.63	1.97
3	6.767	0.013	0.00553	0.075	30.75	99.45	6.73	116.37	1.02
4	6.869	0.013	0.00579	0.316	54.34	98.42	6.76	116.89	1.06
5	6.817	0.010	0.00000	0.278	61.30	98.57	6.72	116.19	2.98
6	6.663	0.010	0.00000	0.000	64.63	99.77	6.65	114.99	1.32
7	6.813	0.009	0.00000	0.010	68.81	99.73	6.79	117.45	5.23
8	6.706	0.015	0.01805	0.000	72.88	99.77	6.69	115.74	1.15
9	6.833	0.012	0.00891	0.000	100.00	99.77	6.82	117.85	0.70
							Total	116.34	1.37
Andros1, J = 0.009901									
1	7.436	0.014	0.00022	4.737	5.45	80.97	6.02	104.45	3.73
2	6.725	0.009	0.09153	0.000	7.76	99.77	6.72	116.15	1.62
3	6.643	0.022	0.01075	0.001	8.27	99.77	6.63	114.68	2.66
4	6.760	0.012	0.00553	0.075	31.18	99.45	6.72	116.25	1.02
5	6.810	0.013	0.00575	0.566	54.79	97.32	6.63	114.67	0.86
6	6.788	0.009	0.00000	0.261	61.73	98.64	6.70	115.79	2.89
7	6.662	0.006	0.00000	0.000	65.01	99.77	6.65	114.98	0.92
8	6.789	0.008	0.00000	0.000	69.17	99.77	6.77	117.1	1.25
9	6.669	0.014	0.00676	0.000	73.20	99.77	6.65	115.1	1.19
10	6.863	0.012	0.00333	0.428	100.00	97.93	6.72	116.22	0.96
							Total	115.64	1.86
Andros1, J = 0.009901									
1	5.834	0.012	0.00000	1.319	5.89	93.05	5.43	94.45	5.54
2	5.444	0.000	0.00000	0.001	6.86	99.71	5.43	94.45	2.32
3	6.410	0.013	0.00314	0.951	56.82	95.38	6.11	106.02	0.85
4	6.093	0.013	0.00000	0.000	71.65	99.74	6.08	105.42	0.8
5	6.025	0.009	0.46843	0.001	72.31	99.74	6.05	104.88	4.4
6	6.139	0.013	0.02646	0.000	81.14	99.75	6.13	106.23	0.88
7	6.518	0.012	0.00036	1.465	100.00	93.12	6.07	105.29	1.37
							Total	105.07	1.34
Andros2, J = 0.009901									
1	4.793	0.018	0.00000	12.844	3.02	20.48	0.98	17.45	4.09
2	1.947	0.012	0.00000	0.827	53.81	86.65	1.69	29.89	0.27
3	1.908	0.013	0.00000	0.933	64.98	84.74	1.62	28.66	1.02
4	1.795	0.013	0.00189	0.476	88.94	91.30	1.64	29.04	0.49
5	1.744	0.011	0.00891	0.033	100.00	98.59	1.72	30.46	1.07
							Total	29.25	0.40
Andros2, J = 0.009901									
1	1.858	0.012	0.02953	3.832	3.94	38.34	0.71	12.68	10.07
2	1.498	0.007	0.00000	0.000	5.81	98.95	1.48	26.29	0.51
3	1.535	0.016	0.03929	0.000	8.51	98.98	1.52	27.00	0.46
4	1.747	0.013	0.01982	0.000	19.8	99.11	1.73	30.7	0.34
5	1.540	0.012	0.00000	0.000	100.00	98.99	1.52	27.03	0.12
							Total	26.88	0.24

grains of phengite in the fraction 0.5–1 mm were dated by laser-probe step heating (see procedure in Monié & Agard, 2009). Leftover single grains were mounted with double-stick conductive carbon tape and analysed with the electron microprobe (8 grains per sample, core and rim analyses). Additionally, one phengite concentrate from Andros2 was dated by ^{40}Ar–^{39}Ar furnace step heating (grain size 0.25–0.5 mm; see procedure in Arnaud *et al.* 2003). The ^{40}Ar–^{39}Ar phengite isotopic data are presented in Tables 3 and 4.

Phengite has been considered for both thermobarometry and geochronology; because this mineral recrystallizes easily, it is stable over a wide range of *P-T* conditions and its composition strongly depends on the *P-T* conditions (Parra, Vidal & Agard, 2002; Vidal *et al.* 2006). Chemical analysis of isolated grains allowed the correlation of pressure–temperature–strain evolution provided by *in situ* petrological and microstructural analysis of thin-sections, as well as ages provided by extracted phengite.

4. *P-T-t* characterization of Makrotantalon unit

4.a. Description of the sample

The glaucophane-garnet schist Andros1 was collected within serpentinite at the base of the Makrotantalon unit (Fig. 1b). The main assemblage contains garnet, phengite, blue amphibole, quartz and rutile (Fig. 2a). The schistosity defined by phengite, blue amphibole and quartz is folded. Garnet has a mosaic texture and contains inclusion of quartz, rutile and phengite. Chloritized biotite is found as a retrogression product after garnet and phengite. Garnet has a homogeneous composition and is very poor in manganese (Fig. 3a, XAlm = 0.62–0.67, XGrs = 0.16–0.24, XPrp = 0.10–0.16, XSps = 0.01–0.03). The blue amphibole is glaucophane of homogeneous and intermediate composition (XMg ~ 0.5, Fig. 3b, c). Two composition clusters are found in both isolated and *in situ* phengite (Fig. 3d): Si-high phengite (XMg ~ 0.6, Si ~ 3.4) and Si-low phengite (XMg ~ 0.65, Si ~ 3.2). In thin-section,

Table 4. $^{40}Ar/^{39}Ar$ phengite isotopic data for the concentrate from the lower unit

Temp	$^{40}Ar/^{39}Ar$	$^{38}Ar/^{39}Ar$	$^{37}Ar/^{39}Ar$	$^{36}Ar/^{39}Ar \times 10^{-3}$	%^{39}Ar released	%$^{40}Ar^*$	$^{40}Ar^*/^{39}Ar_K$	Age (Ma)	$\pm 1\sigma$ (Ma)
Andros2, J = 0.009989									
700	44.448	0.233	0.00005	123.607	0.17	17.79	7.91	137.13	14.49
750	16.36	0.035	0.00207	9.883	0.33	82.05	13.42	227.01	7.21
800	7.305	0.016	0.08161	10.343	0.67	58.03	4.24	74.83	4.42
833	3.983	0.018	0.00066	1.731	1.25	86.77	3.46	61.22	1.16
866	3.070	0.015	0.00932	3.360	2.44	67.18	2.06	36.79	1.33
900	3.170	0.017	0.00216	5.486	4.86	48.37	1.53	27.42	1.05
933	2.302	0.014	0.00000	2.894	12.28	62.17	1.43	25.6	0.33
966	1.704	0.012	0.00268	0.742	18.95	86.22	1.47	26.28	0.23
1000	1.659	0.012	0.00176	0.344	33.05	92.94	1.54	27.58	0.14
1033	1.626	0.012	0.00189	0.143	58.09	96.46	1.57	28.04	0.05
1066	1.542	0.012	0.00264	0.043	83.32	98.18	1.51	27.08	0.05
1100	1.344	0.012	0.00533	0.000	94.41	98.84	1.33	23.78	0.06
1200	1.742	0.014	0.03858	0.888	99.12	84.21	1.47	26.24	0.12
1400	115.207	0.084	0.29585	374.525	100.00	3.94	4.54	80.06	15.64
							Total	28.33	0.36
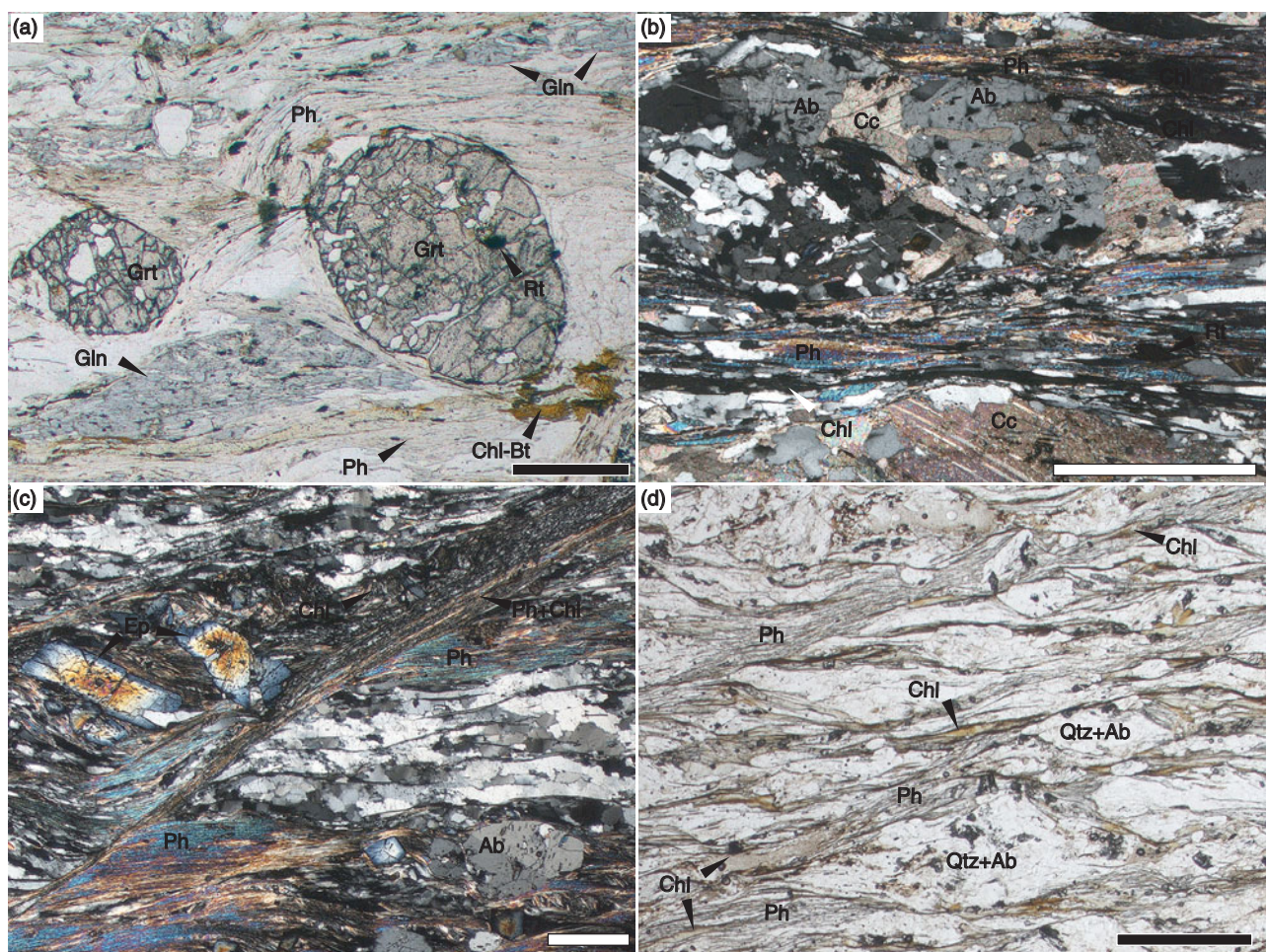
Figure 2. (Colour online) Photomicrographs of the samples. (a) Andros1: the HP-LT equilibrium assemblage contains garnet, glaucophane, phengite and rutile. (b) Andros2: the schistosity is defined by alternating albite-calcite-quartz and phengite-chlorite-quartz layers. (c) Andros 3: the quartz-phengite-epidote-albite-chlorite matrix is cross-cut by a top-to-the-NE shear band containing very-fine-grained phengite, quartz and chlorite. (d) Andros 4: quartz-albite-phengite-chlorite microlithons are separated by a top-to-the-NE extensional crenulation cleavage composed of fine-grained phengite, chlorite and quartz. The thin-sections have been cut in the XZ plane of finite deformation. NE is on the left side of the photos. The scale bars are 500 µm. Mineral abbreviations after Whitney & Evans (2010), except Chl-Bt: chloritized biotite.

Si-high phengite is found both as inclusions and in the matrix and Si-low phengite is found in the matrix. Two of the analysed isolated grains are zoned with a Si-rich core and a Si-poor rim (Fig. 3d). The Si-high phengite is therefore older than the Si-poor phengite.

The compositions of garnet, glaucophane and phengite (Table 1) are similar to those measured in blueschists from the Cyclades (Schliestedt, 1986; Bröcker, 1990; Trotet, Vidal & Jolivet, 2001; Parra, Vidal & Jolivet, 2002). The Si content in phengite
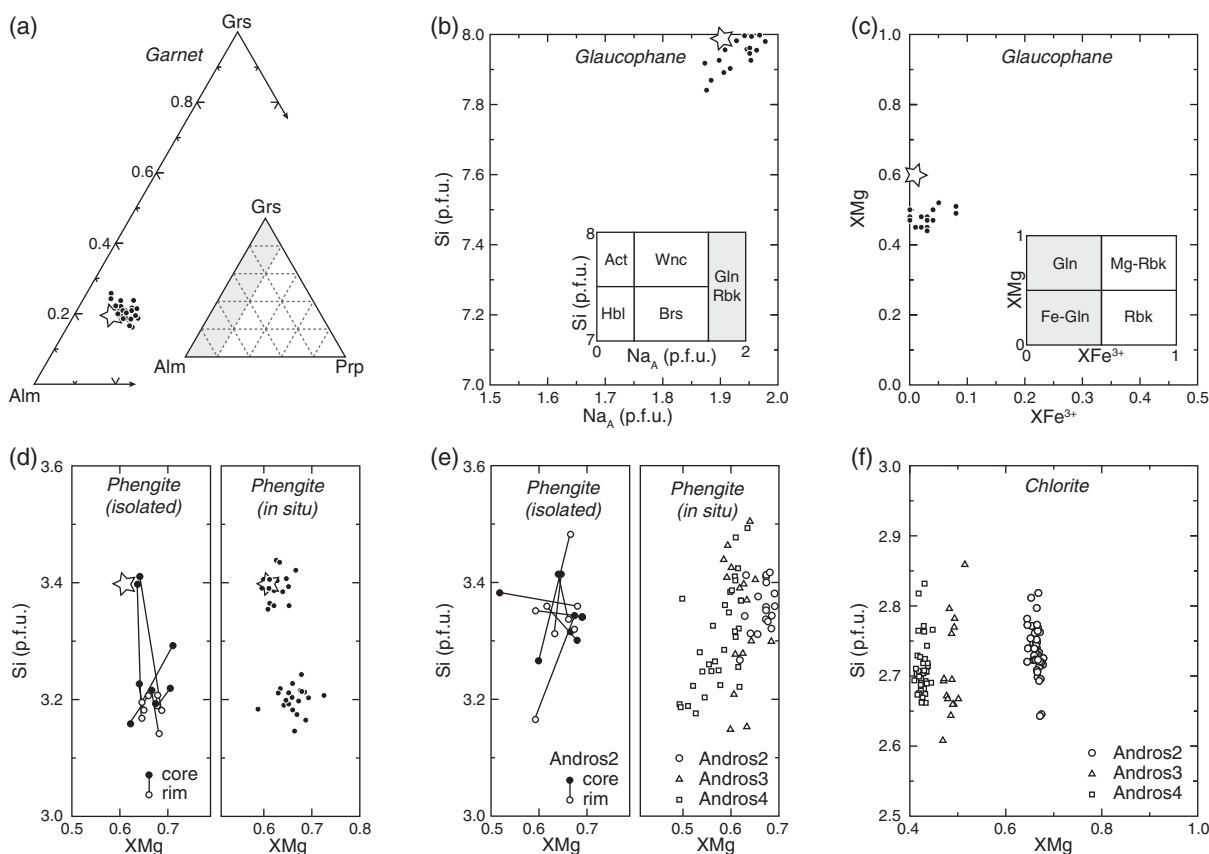
Figure 3. Chemical composition of minerals belonging to the HP-LT paragenesis in (a–d) glaucophane-garnet schist Andros1 and (d, e) phyllosilicates in micaschists Andros2, Andros3 and Andros4. Circles indicate compositions determined with electron microprobe and stars indicate mineral composition modelled at 18.5 kbar and 550 °C. (a) Garnet composition in an Almandine-Grossular-Pyrope ternary diagram. (b, c) Blue amphibole composition in amphibole classification diagrams (Leake *et al.* 2007). (d) Si-XMg diagram of isolated phengite (left panel) and *in situ* phengite (right panel). (e) Si-XMg diagram of isolated phengite (Andros2, left panel) and *in situ* phengite (Andros2, Andros3, Andros4, right panel). (f) Chlorite composition in a Si-XMg diagram. End-member abbreviations after Whitney & Evans (2010).

is controlled by the Tschermak substitution and increases with increasing pressure at constant bulk rock chemistry (Massonne & Schreyer, 1987). We therefore suggest that the Si-high phengite together with garnet, glaucophane and rutile represent the equilibrium HP-LT assemblage in sample Andros1. This assemblage is characteristic of the transition between blueschist and eclogite facies conditions in Ca-poor rocks (Evans, 1990). Si-low phengite and the chloritized biotite are the products of the partial retrogression of this primary assemblage at lower pressure.

4.b. *P-T* estimates

An equilibrium assemblage diagram was calculated (chemical composition in wt%: 0.34 TiO_2, 45.63 Al_2O_3, 29.87 FeO, 6.33 MgO, 5.47 CaO, 2.37 Na_2O and 9.99 K_2O with excess SiO_2 and H_2O). The observed HP-LT equilibrium assemblage is stable within a large field (520–600 °C, 18–22 kbar, Fig. 4a). Comparison between the analysed and modelled chemical compositions of garnet, glaucophane and phengite precisely constrain the *P-T* conditions of the observed

assemblage at 550 °C and 18.5 kbar (stars in Figs 3a–d, 4a). At these conditions the modelled compositions match the analyses within natural scatter, except for the XMg in glaucophane (Fig. 3c).

These conditions fall within the field corresponding to the observed HP-LT assemblage and are considered the peak conditions associated with the HP-LT event recorded in Makrotantalon unit. The observation of chloritized biotite is consistent with an exhumation path first crossing fields where biotite alone is stable and then fields where chlorite replaces it progressively (Fig. 4a).

4.c. ^{40}Ar–^{39}Ar ages

The three dated isolated phengite grains extracted from Andros1 produced age spectra showing no evidence of a major disturbance in the K–Ar system (Fig. 5a–c). The first step or first two steps (less than 7% of the released ^{39}Ar) have a large uncertainty which is associated with a large atmospheric argon component loosely bound to low retentivity sites, such as grain surface. Two grains yielded
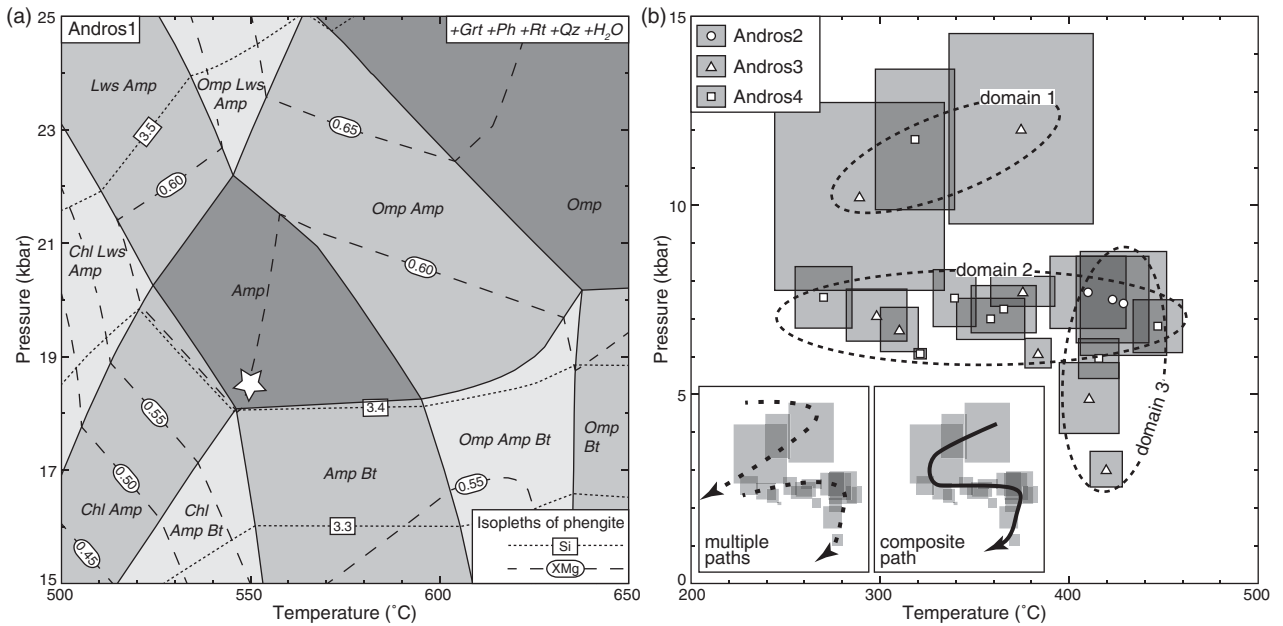
Figure 4. (a) Equilibrium assemblage diagram calculated for glaucophane-garnet schist Andros1 as a function of pressure and temperature. The dotted and dashed lines are isopleths of Si and XMg in the phengite, respectively. Garnet, phengite, rutile, quartz and water being stable at all the conditions covered by the diagram, they are not indicated in the assemblage labelling the different fields. The star indicates the pressure–temperature conditions of peak metamorphism (18.5 kbar and 550 °C). Mineral abbreviations after Whitney & Evans (2010). (b) Pressure–temperature estimates and uncertainties calculated for phengite-chlorite pairs in micaschists Andros2, Andros3 and Andros4.
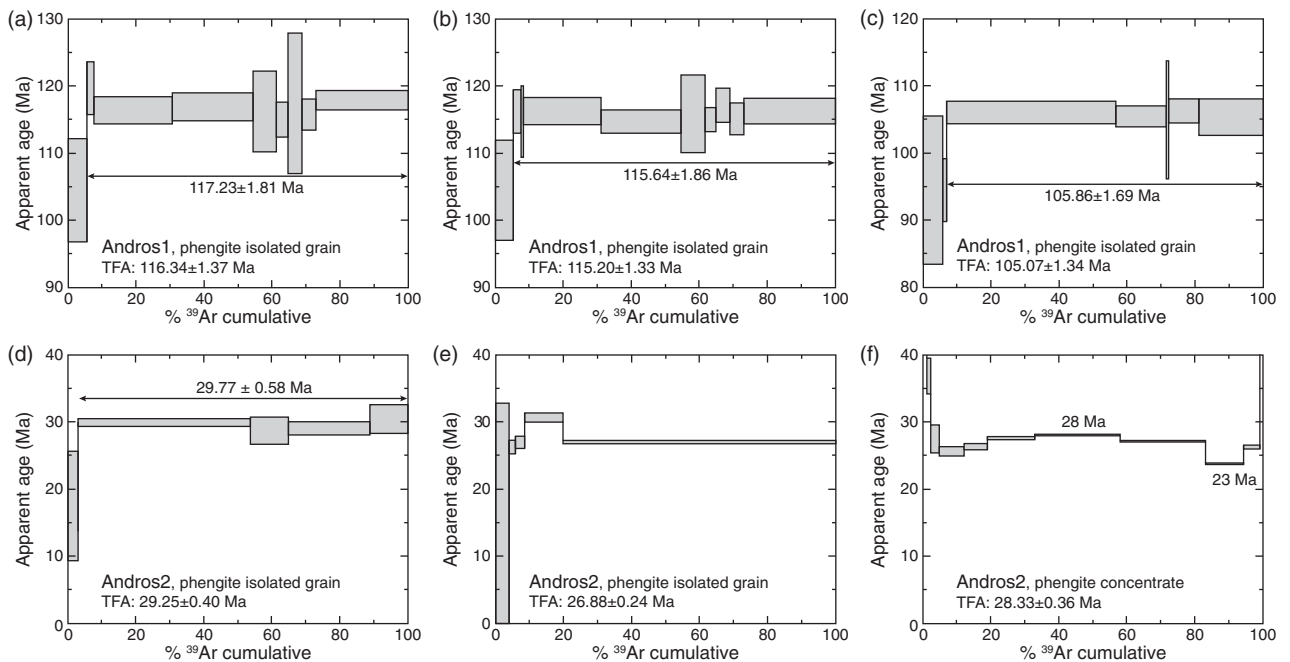
Figure 5. The phengite Ar age spectra (a–c) from glaucophane-garnet schist Andros1 indicate Early Cretaceous ages and (d–f) from micaschist Andros2 indicate Oligo-Miocene ages. The plateau ages, the considered steps for their calculations and the total fusion ages (TFA) are indicated. Steps and calculated ages are provided with a 1σ uncertainty.

2σ-plateau ages for 95% of the released ^{39}Ar that are identical within the uncertainty: 117.2 ± 1.8 Ma and 115.6 ± 1.9 Ma (Fig. 5a, b). A third grain produced a younger 2σ-plateau age (105.9 ± 1.7 Ma, Fig. 5c). This age overlaps with two phengite Rb–Sr ages at 104.6 ± 3.8 Ma and 103.9 ± 1.3 Ma from an albite schist of the Makrotantalon unit (Fig. 6; Bröcker & Franz, 2006; Huyskens & Bröcker, 2014).

4.d. Interpretation of the ^{40}Ar–^{39}Ar ages

These phengite ^{40}Ar–^{39}Ar ages are either reproducible (c. 116 Ma) or confirmed by geochronology with the Rb–Sr system (c. 105 Ma) and the spectra do not show evidence of major disturbance. The concordance of ages determined with the ^{40}Ar–^{39}Ar and another system probably indicates that excess argon is not a major problem in the dated sample, as it has been
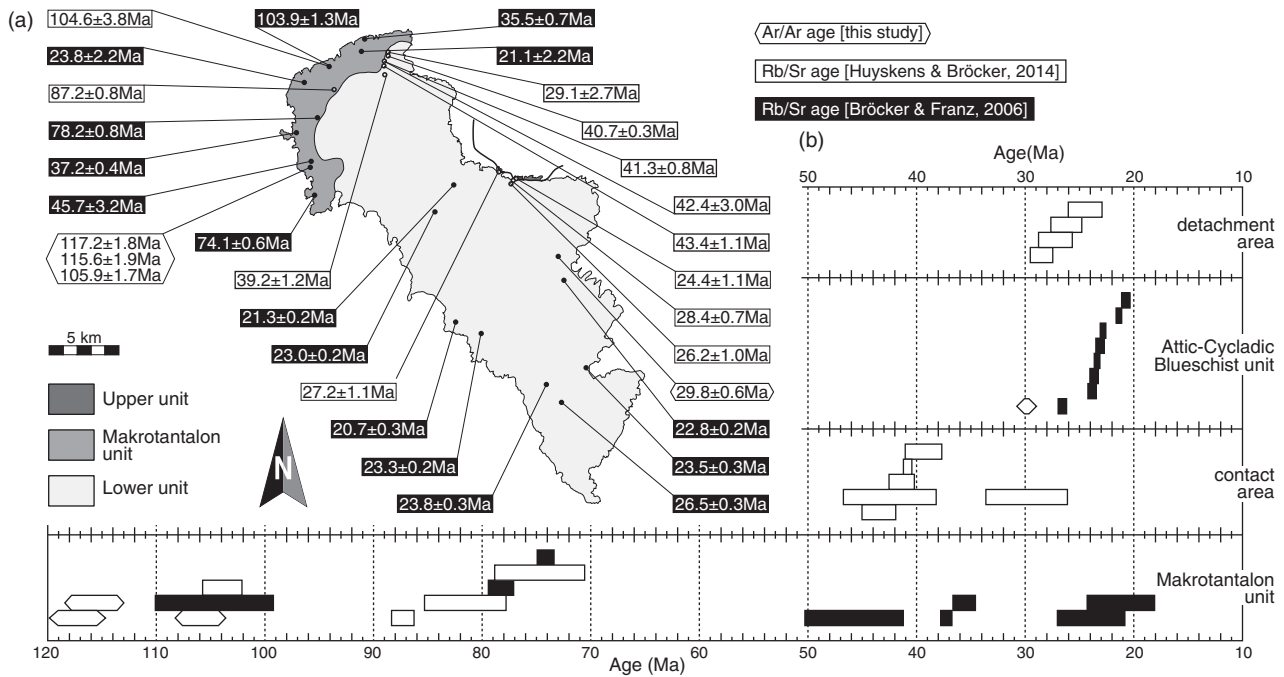
Figure 6. Space and time distribution of the radiochronologic ages from Andros on (a) a map and (b) a time scale.

demonstrated in other HP belts such as the d'Entrecasteaux belt of Papua New Guinea (Baldwin *et al.* 1993, 2004; Baldwin, Webb & Monteleone, 2008). In general, excess argon is limited to polyorogenic belts where old protoliths are poorly deformed, partially recrystallized and with limited fluid circulation (Schneider *et al.* 2007). Solid diffusion modelling (Warren, Hanke & Kelley, 2012) using recent diffusion parameters (Harrison *et al.* 2009) suggests that the K–Ar system in white mica has a higher closure temperature (500–550 °C) than generally accepted, especially at high pressure, as suggested by previous studies (Lister & Baldwin, 1996; Villa, 1998). Finally, phengite ^{40}Ar–^{39}Ar geochronology using *in situ* methods suggests that argon diffusion can be negligible even at relatively high temperatures (Di Vincenzo *et al.* 2001; Agard *et al.* 2002; Maurel *et al.* 2003; Mulch & Cosca, 2004; Augier *et al.* 2005). The ages determined in sample Andros1 are therefore considered as geologically relevant crystallization ages because of the similarity between the recorded peak temperature in sample Andros1 and the closure temperature for Ar in white mica.

In sample Andros1, two different phengite chemistries have been recognized. Si-high phengite crystallized at peak conditions and Si-low phengite crystallized later during retrogression. Two different ages (*c.* 116 and 105 Ma) have been determined in this sample, interpreted as crystallization ages. We cannot provide proof of direct correspondence between the phengite chemistry and the ages, and therefore assume that each phengite growth step is associated with one age. We therefore suggest that the 116 Ma age dates the peak conditions or the onset of exhumation right after maximum burial, whereas the 105 Ma age corresponds to a step along the retrogression path. This indic-

ates a short residence time at temperatures higher than 500 °C, consistent with negligible Ar loss in the investigated large grains (Warren, Hanke & Kelley, 2012).

5. *P-T-t* characterization of the Attic–Cycladic Blueschist unit

5.a. Description of samples

The micaschists Andros2, Andros3 and Andros4 have been sampled at different structural levels and in different structures of the Attic–Cycladic Blueschist unit (Fig. 1b). Andros2 has been sampled in a boudin preserved from late deformation. Its microstructure is dominated by a single schistosity (Fig. 2b). In contrast, Andros3 and Andros4 have been sampled in zones of intense top-to-the-NE ductile deformation at a higher structural level closer to the detachment (Fig. 1b). They exhibit shear-bands deflecting the schistosity (Fig. 2c, d). All contain phengite, chlorite, albite and quartz. Additional minerals are calcite and rutile in Andros2 and epidote in Andros3.

In all samples, phengite and chlorite show wide ranges of Si-content (Phg:Si = 3.15–3.52, Chl:Si = 2.6–2.9) and clustered XMg values (Fig. 3e, f; Table 1). Similar variations have been observed in the phyllosilicates of the neighbouring island of Tinos (Parra, Vidal & Jolivet, 2002). Sample Andros2 shows a slightly larger dispersion in analysis performed on isolated grains compared to *in situ* measurements (Fig. 3e).

For a constant bulk-rock chemistry, Si variations in phengite indicate variable crystallization pressures (Massonne & Schreyer, 1987). Similarly, the Si variations in chlorite are correlated with variation of crystallization temperature (Vidal, Parra & Trotet, 2001).

The observed chemical variations within each sample reflect crystallization at different conditions. The range of Si in the phengite is narrower in Andros2 than in the other micaschists, most probably reflecting a narrower range of crystallization pressure conditions recorded in this sample.

5.b. *P-T* estimates

The distribution of the *P-T* estimates determined by multi-equilibrium thermobarometry in the micaschists is complex (Fig. 4b). Different *P-T* conditions are determined in the same sample and the *P-T* record is heterogeneous. Sample Andros4 yielded two types of *P-T* estimates. One *P-T* estimate is situated at 320 °C and 12 kbar, whereas the seven others have a similar pressure (*c.* 7 kbar) but different temperatures covering a wide range (260–430 °C). The latter plot a plateau at constant pressure. Pressure–temperature estimates determined in sample Andros3 confirm either the HP-LT record or the plateau at 7 kbar. These two samples from the same structural level share a common *P-T* history. Further, two other *P-T* estimates from sample Andros3 are situated at the maximum temperature of the plateau and lower pressure. Sample Andros2 yielded one cluster of *P-T* conditions located at the high-temperature part of the plateau. This record is consistent with the deeper structural position of the sample, its monophase structure and the rather homogeneous composition of phyllosilicates.

Even though there is clear evidence for deformation within the Attic–Cycladic Blueschist unit, there is no major internal shear zone (Mehl *et al.* 2007). This unit is apparently coherent and it is legitimate to define a single composite *P-T* path rather than multiple paths (insets of Fig. 4b). Three *P-T* domains are distinguished. Domain 1 corresponds to estimates determined in samples Andros3 and Andros4 with pressure above 10 kbar and temperature in the range 300–400 °C. The uncertainty is important, which might reflect partial re-equilibration of the initial mineral chemistry in the following stages of the *P-T* path. Domain 1 constrains the *P-T* path in HP-LT conditions. Domain 2 corresponds to estimates determined in the three micaschists with temperature in the range 260–430 °C for *c.* 7 kbar. This domain indicates heating at constant pressure. Domain 3 corresponds to estimates determined in the three micaschists with pressure below 7 kbar for *c.* 400 °C. Domain 3 constrains the *P-T* path in the greenschist facies. Notice that the *P-T* estimates yielded by sample Andros2 are in both domains 2 and 3. The *P-T* conditions in domains 2 and 3 are consistent with most of those determined in mafic greenschists of the Attic–Cycladic Blueschist unit (Fig. 7a; Bröcker & Franz, 2006).

5.c. $^{40}Ar–^{39}Ar$ ages

One isolated grain of sample Andros2 yielded a 2σ-plateau age at 29.8 ± 0.6 Ma determined for 97% of the released ^{39}Ar (Fig. 5d). The first step has a large uncertainty, which is associated with a large atmospheric argon component trapped in lesser retentive sites such as the grain surface. No other major disturbance in the K–Ar system can be inferred from this spectrum. Another single grain produced a discordant spectrum for which no plateau can be defined (Fig. 5e), since *c.* 80% of ^{39}Ar was released in a single step. A concentrate produced a perturbed spectrum (Fig. 5f). The global U-shaped pattern reveals Ar excess degassed at low and high experimental temperatures. The convex-downwards central part is consistent with mixing of two phengite populations (Wijbrans & McDougall, 1986). The scatter in phengite composition supports this interpretation (Fig. 3e). A younger bound for the age of the older population would be 28 Ma and an older bound for the age of the younger population would be 23 Ma (Fig. 5f). The older bound is consistent with the single-grain plateau age of 29.8 ± 0.6 Ma and an Rb–Sr phengite age of 29.1 ± 2.7 Ma (Fig. 6; Huyskens and Bröcker, 2014), and the younger bound is consistent with seven Rb–Sr phengite ages in the range 21–24 Ma (Fig. 6; Bröcker & Franz, 2006).

5.d. Interpretation of the $^{40}Ar–^{39}Ar$ ages

These $^{40}Ar–^{39}Ar$ ages have been determined in phengite that apparently crystallized at 400–430 °C and *c.* 7 kbar (Fig. 4b). The *P-T* estimates of domain 3 show no evidence of further heating. The plateau age at 29.8 ± 0.6 Ma, for which no mixing and no perturbation of the argon system are recognized, is therefore considered as a crystallization age. This age overlaps with a phengite Rb–Sr age at 29.1 ± 2.7 Ma (Fig. 6; Huyskens & Bröcker, 2014). It dates the *P-T* conditions recorded in sample Andros2, which correspond to the end of the isobaric heating and the onset of exhumation in the greenschist facies.

6. Discussion

We here combine our pressure–temperature and time constraints with data from the literature in order to build the *P-T-t* paths of both the Attic–Cycladic Blueschist and Makrotantalon units and discuss their implications.

6.a. The *P-T-t* path of the Attic–Cycladic Blueschist unit on Andros

Since more information about the *P-T-t* evolution of the Attic–Cycladic Blueschist unit is available, it is discussed first. The available peak *P-T* conditions for this unit are 450–500 °C and minimum pressure of 10 kbar (Reinecke, 1986). Following Bröcker & Franz (2006), we use peak data from Tinos island – 500–520 °C and 16–18 kbar (Parra, Vidal & Jolivet, 2002) – which is compatible with the wider peak range of 450–550 °C and 12–20 kbar (Fig. 7a) determined by Bröcker (1990). The end of the exhumation under HP-LT conditions is constrained by the *P-T* estimates of
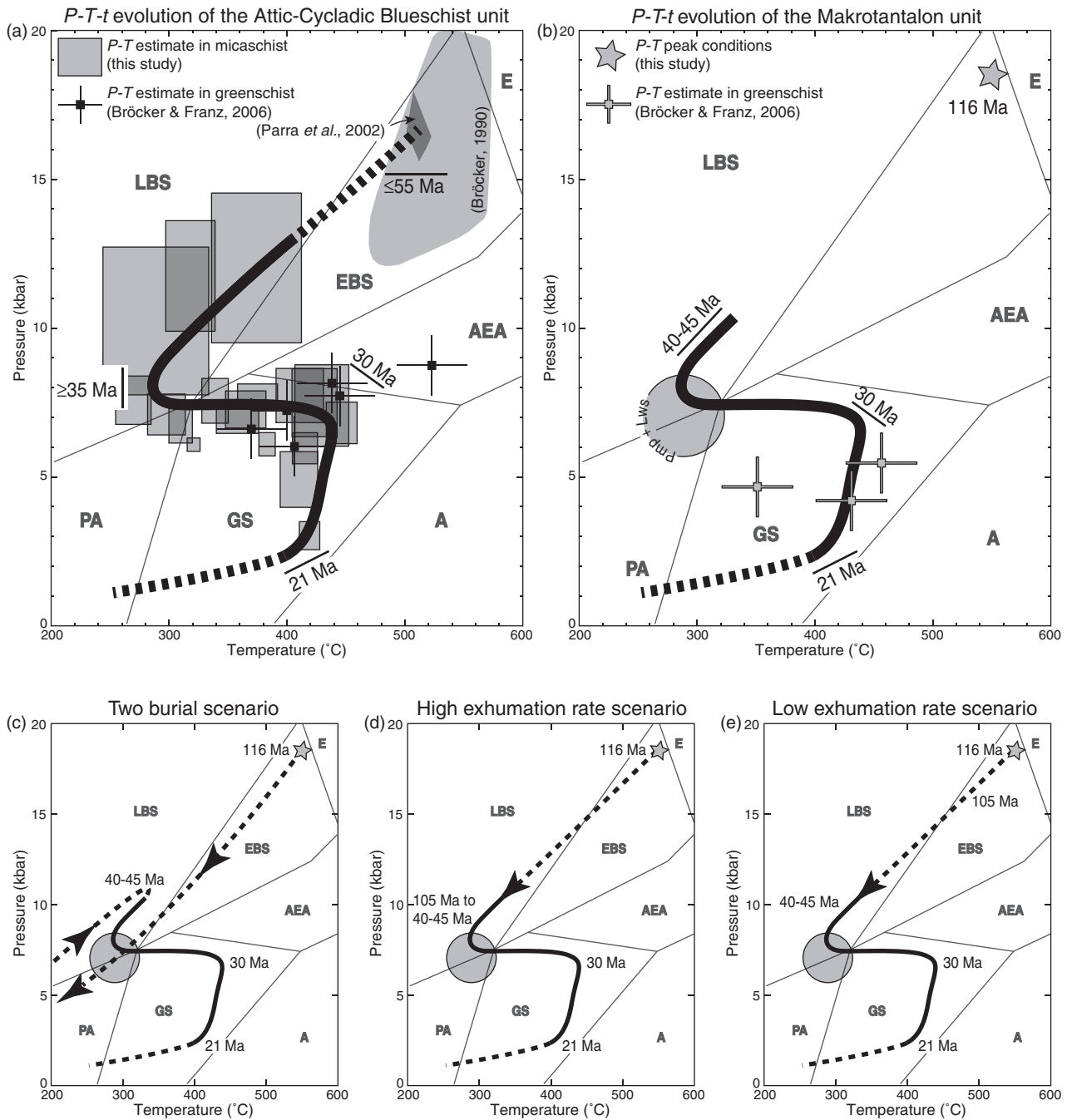
Figure 7. Pressure–temperature–time evolution of the (a) Attic–Cycladic Blueschist unit and (b) Makrotantalon unit on Andros. *P-T* conditions estimated in greenschists are taken from Bröcker & Franz (2006). The range of peak conditions in Tinos (Bröcker, 1990; Parra, Vidal & Jolivet, 2002) is taken as a proxy for the peak conditions in the Attic–Cycladic Blueschist unit. (c–e) Three possible *P-T-t* histories for the Makrotantalon unit.

group 1 (Fig. 7a; see Section 5.b), stopping at *c.* 300 °C and 7 kbar. By comparison with the well-documented areas of the Attic–Cycladic Blueschist, this HP-LT exhumation can be bracketed between 35 Ma and 55 Ma (Jolivet & Brun, 2010). The peak is then younger than 55 Ma and conditions of 300 °C and 7 kbar are reached before 35 Ma.

Exhumation under HP-LT conditions is then followed by heating at constant 7 kbar pressure up to 420 °C, as shown by *P-T* estimates of group 2 (Fig. 7a). *P-T* estimates of group 3 indicate nearly isothermal decompression at 400–420 °C between 7 and 2 kbar.

The onset of this second period of exhumation is constrained by our phengite ^{40}Ar–^{39}Ar plateau age of *c.* 30 Ma. The almost continuous geochronologic record by the phengite Rb–Sr method (Fig. 6) shows that it occurred between 30 Ma and 21 Ma. This is consistent with the discordant phengite ^{40}Ar–^{39}Ar spectra obtained in this study (Fig. 5f), which is interpreted as the effect of a phengite mixture between a population older than 28 Ma and a population younger than 23 Ma. The youngest phengite Rb–Sr age at 21 Ma is likely to date the end of ductile deformation at 350–400 °C.

6.b. Possible *P-T-t* paths for the Makrotantalon unit

Our results constrain the HP-LT peak conditions in the Makrotantalon unit at 550 °C, 18.5 kbar and 116 Ma (Fig. 7b). We suggest that this correlates with the Early Cretaceous blueschist metamorphism described in the Pelagonian region of continental Greece. The later evolution of the Makrotantalon unit is constrained by phengite Rb–Sr and ⁴⁰Ar–³⁹Ar ages and petrologic observations that are not tightly linked together.

1. The *P-T* conditions related to the 105 Ma re-equilibration are not known, but are most likely at lower grade than the peak conditions.

2. The phengite Rb–Sr ages between 70 and 90 Ma (Fig. 6; Bröcker & Franz, 2006; Huyskens & Bröcker, 2014) are the record of a metamorphic event that is contemporaneous with a widespread metamorphism and plutonism in Pelagonian unit (Patzak, Okrusch & Kreuzer, 1994). This supports a Pelagonian origin for the Makrotantalon unit (Bröcker & Franz, 2006; Huyskens & Bröcker, 2014), but additional investigations are required to characterize the degree of thermal overprint related to this episode.

3. The phengite Rb–Sr ages in the contact area between the Makrotantalon and the Attic–Cycladic Blueschist units cluster at 40–45 Ma, which could date the stacking between the two units (Fig. 6; Huyskens & Bröcker, 2014). According to these ages, the Makrotantalon unit was stacked on top of the Attic–Cycladic Blueschist unit during Eocene time while the latter was still experiencing HP-LT conditions and exhuming in the subduction zone below the Pelagonian unit that represented the upper plate (Trotet, Jolivet & Vidal, 2001; Jolivet *et al.* 2012; Philippon, Brun & Gueydan, 2012). The Makrotantalon unit can therefore be considered as part of the upper plate of the subduction zone until 40–45 Ma, and its basal contact was not a thrust (Huyskens & Bröcker, 2014) but a normal fault. The *P-T* conditions at which the two units were finally stacked together are of *T* > 300 °C and *P* > 7 kbar. The Makrotantalon unit therefore followed the same *P-T-t* path as the Attic–Cycladic Blueschist unit after 40–45 Ma (Fig. 7b). This is consistent with two of the three *P-T* estimates in greenschists (Bröcker & Franz, 2006).

4. The assemblages containing albite, lawsonite and pumpelleyite without glaucophane (Huyskens & Bröcker, 2014) indicate that at least part of the Makrotantalon unit equilibrated at the boundary between the pumpelleyite-albite and the lawsonite blueschist facies. Petrological grids constrain this equilibration at *c.* 300 °C and 7 kbar (Fig. 7b; Evans, 1990), which corresponds (fortuitous or not) to the final HP-LT exhumation in the Attic–Cycladic Blueschist unit (Fig. 7a).

5. A wide range of meaningful Rb–Sr and ⁴⁰Ar–³⁹Ar ages and *P-T* conditions is preserved. A first interpretation is that the Makrotantalon unit is a tectonic mélange containing elements with different metamorphic histories. Alternatively, it indicates that both isotopic and petrologic systems have barely been perturbed at high temperature. We consider the first explanation as unlikely, since the distinctive Permian marble layer can be followed over several kilometres (Fig. 1b).

Based on these constraints and assuming that the Makrotantalon unit was coherent, we propose three possible *P-T-t* paths between 116 Ma and 40–45 Ma (Fig. 7c–e). The first scenario considers rapid post-peak exhumation of the Makrotantalon unit close to the surface (Fig. 7c). Low-pressure re-equilibration at 105 Ma would occur along this exhumation. The unit would then have been buried again and stacked with the Attic–Cycladic Blueschist unit in HP-LT conditions at 40–45 Ma, close to conditions where lawsonite and pumpelleyite are co-stable. There is no direct evidence of shallow exhumation of the Makrotantalon unit. However, Late Cretaceous and Paleocene flysch deposited above the Pelagonian unit contains detrital glaucophane (Faupl, Pavlopoulos & Migiros, 1999; Faupl *et al.* 2002), indicating that blueschist-facies rocks were at the surface and eroded as early as *c.* 100 Ma (Faupl *et al.* 2002). The Makrotantalon unit, or one of its lateral equivalent, could be the source of this detrital glaucophane. The second scenario considers rapid post-peak exhumation up to conditions where lawsonite and pumpelleyite are both stable (Fig. 7d). The Makrotantalon would then have been at stable *P-T* conditions in the hanging wall of the Hellenic subduction zones until partial exhumation of the Attic–Cycladic Blueschist unit over which it stacked at 40–45 Ma. The *P-T* evolution in the third scenario is similar (Fig. 7e), but the Makrotantalon exhumed slowly until stacking over the Attic–Cycladic Blueschist unit. This scenario implies long residence time at high temperature and is not entirely consistent with limited isotopic resetting.

6.c. Implications for the history of the Hellenic subduction zone

The HP-LT paragenesis described on Makrotantalon belongs, at least partly, to the Eohellenic phase. It is synchronous with the obduction of the Othrys ophiolite (110–130 Ma; Jacobshagen, 1986) and the initiation of blueschist facies metamorphism in the Pelagonian unit (see Fig. 1a) at 100–125 Ma in the Ossa range (Lips, White & Wijbrans, 1998) and at 110–120 Ma on Evia island (Maluski *et al.* 1981). The onset of blueschist facies metamorphism in the Olympos range could be younger (at least 100 Ma; Schermer, 1990; Schermer, Lux & Burchfiel, 1990). This episode in continental Greece is closer to greenschist facies/blueschist facies transition (Schermer, 1990; Schermer, Lux & Burchfiel, 1990; Lips, White & Wijbrans, 1998), that is, lower grade than the Makrotantalon unit on Andros. This Cretaceous event is younger than the Late Jurassic obduction of the Vourinos ophiolite and older than the obduction of Late Cretaceous Vardar–Izmir–Ankara ophiolite and the final closure of the Tethys Ocean. It confirms a continuous subduction and accretion in the Vardar–Izmir–Ankara suture zone south of the Rhodope since Early Cretaceous time.

These Early Cretaceous peak conditions in the Makrotantalon unit are similar to the Eocene peak conditions determined in the Attic–Cycladic Blueschist unit (see a review in Philippon, Brun & Gueydan, 2012). This may imply that the Hellenic subduction zone could have been at thermal steady state during Early Cretaceous – Eocene time. Exhumation of the HP-LT rocks in the subduction zone would have been a short-lived discontinuous phenomenon related to Early Cretaceous obduction and Eocene accretion of continental terrain. Such behaviour is consistent with a worldwide review of the dynamics of oceanic subduction zones (Agard *et al.* 2009).

6.d. Implications for the evolution of the North Cycladic Detachment System

The North Cycladic Detachment System (NCDS) acted as a normal fault exhuming the Attic–Cycladic Blueschist unit in the northern part of this unit (Jolivet *et al.* 2010). It controlled both syn-orogenic (in the Hellenic subduction zone) and post-orogenic (in the back-arc of the Hellenic subduction zone) exhumation.

Figure 8a depicts the compiled *P-T-t* paths of the Attic–Cycladic Blueschist in the NCDS footwall: Olympos range (Schermer, 1990; Schermer, Lux & Burchfiel, 1990); Ossa/Pelion range (Lips, White & Wijbrans, 1998; Lips, Wijbrans & White, 1999; Lacassin *et al.* 2007); Evia island (Katzir *et al.* 2000; Ring *et al.* 2010); Andros island (this study); and Tinos island (Parra, Vidal & Jolivet, 2002). Along-strike from NW to SE (Olympos, Ossa/Pelion, Evia, Andros, Tinos; Fig. 1a), conditions of Eocene HP-LT metamorphism and the maximum temperature during Oligo-Miocene exhumation both increase below the NCDS. This trend highlights a gradient of exhumation along the NCDS, where the deepest and warmest rocks are exhumed in the centre of the Aegean (Jolivet & Patriat, 1999). Furthermore, two groups of *P-T-t* evolution can be distinguished. In continental Greece and on Evia Island decompression is accompanied by constant cooling, whereas in the Cyclades there is a break in exhumation accompanied with heating at constant pressure. The timing (before *c.* 37–30 Ma) and amount of heating (100–150 °C) on each island is similar. This corresponds to thermal re-equilibration of the lithosphere between a cold syn-orogenic regime in the subduction zone and a warm post-orogenic regime in the back-arc of the subduction zone (Parra, Vidal & Jolivet, 2002), and coincides with a change of boundary conditions due to the onset of slab retreat (Jolivet & Faccenna, 2000). Pressure of this thermal excursion (7 kbar on Andros and 9 kbar on Tinos) indicates that thermal re-equilibration occurred at lower crustal depth.

Four detachments have been identified in the North Cycladic Detachment System (Fig. 8b; Jolivet *et al.* 2010) as follows. (1) The Vari detachment (observed on Syros and Tinos) is an Eocene ductile low-angle normal fault active in the Hellenic subduction zone under HP-LT conditions. It was partly reactivated at 10 Ma.
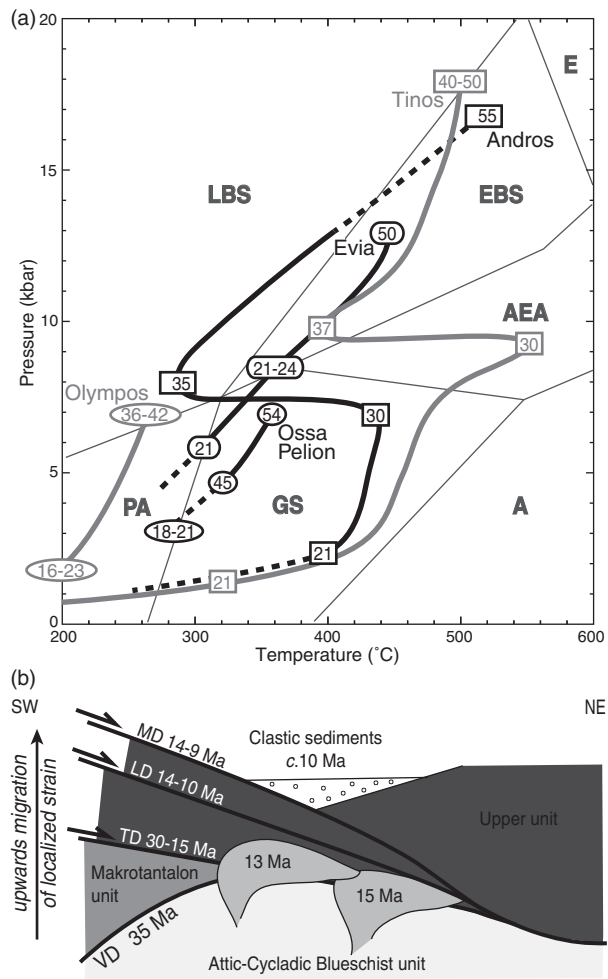

Figure 8. (a) Pressure–temperature–time path of the NCDS hanging wall in Olympos (Schermer, 1990; Schermer, Lux & Burchfiel, 1990), Ossa-Pelion (Lips, White & Wijbrans, 1998; Lips, Wijbrans & White, 1999; Lacassin *et al.* 2007), SE Evia (Katzir *et al.* 2000; Ring *et al.* 2010), Andros (this study) and Tinos (Parra, Vidal & Jolivet, 2002). (b) Schematic cross-section indicating the upwards migration of localized strain in the NCDS.

(2) The Tinos detachment (observed on Andros and Tinos) is an Oligo-Miocene (15–30 Ma) brittle–ductile low-angle normal fault. It localizes at the bottom of the upper unit. (3) The Livada detachment (observed on Tinos and Mykonos) is a low-angle brittle–ductile normal fault (14–10 Ma). It deforms syn-tectonic I-type granitoids which are 14–15 Ma old on Tinos (Altherr *et al.* 1982; Avigad & Garfunkel, 1989; Bröcker & Franz, 1994; Brichau *et al.* 2007) and 13 Ma old on Mykonos (Altherr *et al.* 1982; Brichau *et al.* 2008) and localizes within the upper unit above these intrusions. (4) The Mykonos detachment is a low-angle brittle normal fault localizing in the upper unit and at the bottom of Miocene clastic sediments (Lecomte *et al.* 2010), and was active between 14 and 9 Ma. All these detachment have a top-to-the-N or -NE kinematics.

Based on similar structural position and timing, we correlate the contact at the bottom of the Makrotantalon unit with the Vari detachment. Incorporation of the Makrotantalon unit within the Attic–Cycladic

Blueschist at 40–45 Ma suggests that this unit moved from the hanging wall of the NCDS to its footwall during syn-orogenic exhumation. Localized strain in the NCDS jumped structurally higher in the Tinos detachment (at the bottom of the Pelagonian ophiolite), the activity of which was constrained by phengite Rb–Sr ages of 24–28 Ma (Huyskens & Bröcker, 2014). This jump is coeval with the thermal re-equilibration that occurred before 35–30 Ma. We suggest that this jump is controlled by both uplifting of the brittle–ductile transition (Jolivet *et al.* 2010) and strong strength contrasts at the bottom of the Pelagonian ophiolite (Huet *et al.* 2011*a*, *b*). Localized strain has again migrated upward within the NCDS: in the Livada detachment and in the Mykonos detachment (Fig. 8b, Jolivet *et al.* 2010). In both cases, migration is controlled by successive uplifting of the brittle–ductile transition favoured by intrusion of warm material.

Active deformation in the NCDS has therefore always migrated upward and each uplift event can be related to a perturbation of the thermal state in the crust. These brutal migrations of the localized strain are consistent with the predictions of thermomechanical models showing that long-lived detachment zones are made of anastomosed shear zones, which are active at different times of the activity of the detachment (Huet *et al.* 2011*a*, *b*). We therefore suggest that deformation in a long-lived crustal-scale normal fault tends to migrate upwards; this is contrary to a thrust, in which case it migrates downwards.

7. Conclusion

Phengite ⁴⁰Ar–³⁹Ar geochronology coupled with thermobarometry is a powerful method that allows the tectono-metamorphic evolution of Andros Island to be determined. The Makrotantalon unit experienced HP-LT metamorphism with peak conditions at 550 °C and 18.5 kbar at 116 Ma. This correlates with Early Cretaceous blueschist facies metamorphism in the Pelagonian area of continental Greece and favours a Pelagonian origin for the Makrotantalon unit. This unit is now present as a Pelagonian sliver, stacked over to the Attic–Cycladic Blueschist in the Hellenic subduction zone at 40–45 Ma. The *P-T* evolution of the Attic–Cycladic Blueschist unit is characterized by an exhumation after peak conditions under HP-LT conditions at 55–35 Ma, isobaric heating at 7 kbar until 30 Ma and then isothermal decompression until 21 Ma. These *P-T-t* evolutions confirm that transition between a stable regime with thermal steady state and a retreating regime in the Hellenic subduction zone occurred between 35 and 30 Ma. It also confirms that the NCDS is a complex structure in which active deformation migrated upwards, favoured by uplifting of the brittle–ductile transition and controlled by thermal perturbations. This study highlights that *P-T* estimates tightly linked to radiochronology are essential for understanding complex tectono-metamorphic evolutions.

References

AGARD, P., MONIÉ, P., JOLIVET, L. & GOFFÉ, B. 2002. Exhumation of the Schistes Lustrés complex: in situ laser probe ⁴⁰Ar/³⁹Ar constraints, and implications for the Western Alps. *Journal of Metamorphic Geology* **20**, 599–618.

AGARD, P., YAMATO, P., JOLIVET, L. & BUROV, E. 2009. Exhumation of oceanic blueschists and eclogites in subduction zones: Timing and mechanisms. *Earth-Science Reviews* **92**, 53–79.

ALTHERR, R., KREUZER, H., WENDT, I., LENZ, H., WAGNER, G. A., KELLER, J., HARRE, W. & HÖHNDORF, A. 1982. A late Oligocene/early Miocene high temperature belt in the Attic-Cycladic Crystalline Complex (SE Pelagonian, Greece). *Geologisches Jahrbuch* **23**, 97–164.

ALTHERR, R., SCHLIESTEDT, M., OKRUSCH, M., SEIDEL, E., KREUZER, H., HARRE, W., LENZ, H., WENDT, I. & WAGNER, G. A. 1979. Geochronology of high-pressure rocks on Sifnos (Cyclades, Greece). *Contributions to Mineralogy and Petrology* **70**, 245–55.

ARNAUD, N., TAPPONNIER, P., ROGER, F., BRUNEL, M., SCHARER, U., WEN, C. & ZHIQIN, X. 2003. Evidence for Mesozoic shear along the western Kunlun and Altyn-Tagh fault, northern Tibet (China). *Journal of Geophysical Research: Solid Earth* **108**(B1), doi:10.1029/2001JB000904.

AUGIER, R., AGARD, P., MONIÉ, P., JOLIVET, L., ROBIN, C. & BOOTH-REA, G. 2005. Exhumation, doming and slab retreat in the Betic Cordillera (SE Spain): in-situ ⁴⁰Ar/³⁹Ar ages and P-T-d-t paths for the Nevado-Filabride complex. *Journal of Metamorphic Geology* **23**, 357–81.

AVIGAD, D. & GARFUNKEL, Z. 1989. Low-angle faults above and below a blueschist belt: Tinos Island, Cyclades, Greece. *Terra Nova* **1**, 182–7.

AVIGAD, A., GARFUNKEL, Z., JOLIVET, L. & AZAÑÓN, J. M. 1997. Back-arc extension and denudation of Mediterranean eclogites. *Tectonics* **16**, 924–41.

BALDWIN, S. L., LISTER, G. S., HILL, E., FOSTER, D. A. & McDOUGALL, I. 1993. Thermochronologic constraints on the tectonic evolution of active metamorphic core complexes, D'Entrecasteaux Islands, Papua New Guinea. *Tectonics* **12**(3), 611–28.

BALDWIN, S. L., MONTELEONE, B. D., WEBB, L. E., FITZGERALD, P. G., GROVE, M. & HILL, E. J. 2004. Pliocene eclogite exhumation at plate tectonic rates in eastern Papua New Guinea. *Nature* **431**(7006), 263–7.

BALDWIN, S. L., WEBB, L. E. & MONTELEONE, B. 2008. Late Miocene coesite-eclogite exhumed in the Woodlark Rift. *Geology* **36**(9), 735–8.

BERMAN, R. G. 1991. Thermobarometry using multi-equilibrium calculations: a new technique, with petrological applications. *Canadian Mineralogist* **29**, 833–55.

BONNEAU, M. 1984. Correlation of the Hellenic nappes in the south-east Aegean and their tectonic reconstruction. In *The Geological Evolution of the Eastern Mediterranean* (eds J. E. Dixon & A. H. F. Robertson), pp. 517–27. Geological Society of London, Special Publication no. 17.

BRICHAU, S., RING, U., CARTER, A., BOLHAR, R., MONIE, P., STOCKLI, D. & BRUNEL, M. 2008. Timing, slip rate, displacement and cooling history of the Mykonos

detachment footwall, Cyclades, Greece, and implications for the opening of the Aegean Sea basin. *Journal of the Geological Society of London* **165**, 263–77.

BRICHAU, S., RING, U., CARTER, A., MONIE, P., BOLHAR, R., STOCKLI, D. & BRUNEL, M. 2007. Extensional faulting on Tinos Island, Aegean Sea, Greece; how many detachments? *Tectonics* **26**, TC4009.

BRÖCKER, M. 1990. Blueschist-to-greenschist transition in metabasites from Tinos island, Cyclade, Greece: compositional control or fluid infiltration. *Lithos* **25**, 25–39.

BRÖCKER, M. & ENDERS, M. 1999. U-Pb zircon geochronology of unusual eclogite-facies rocks from Syros and Tinos (Cyclades, Greece). *Geological Magazine* **136**, 111–8.

BRÖCKER, M. & ENDERS, M. 2001. Unusual bulk-rock compositions in eclogite-facies rocks from Syros and Tinos (Cyclades, Greece): implications for U-Pb zircon geochronology. *Chemical Geology* **175**, 581–603.

BRÖCKER, M. & FRANZ, L. 1994. The contact aureole on Tinos (Cyclades, Greece). Part I: field relationships, petrography and P-T conditions. *Chemie der Erde* **54**, 262–80.

BRÖCKER, M. & FRANZ, L. 1998. Rb-Sr isotope studies on Tinos Island (Cyclades, Greece): additional time constraints for metamorphism, extent of infiltration-controlled overprinting and deformational activity. *Geological Magazine* **135**, 369–82.

BRÖCKER, M. & FRANZ, L. 2006. Dating metamorphism and tectonic juxtaposition on Andros Island (Cyclades, Greece): results of a Rb-Sr study. *Geological Magazine* **143**, 609–20.

BRÖCKER, M., KREUZER, H., MATTHEWS, A. & OKRUSCH, M. 1993. ^{40}Ar/^{39}Ar and oxygen isotope studies of polymetamorphism from Tinos island, Cycladic blueschist belt, Greece. *Journal of Metamorphic Geology* **11**, 223–40.

BRÖCKER, M. & PIDGEON, R. T. 2007. Protolith ages of metaigneous and meta-tuffaceous rocks from the Cycladic blueschist unit, Greece: results of a reconnaissance U-Pb zircon study. *Journal of Geology* **115**, 83–98.

BULLE, F., BRÖCKER, M., GÄRTNER, C. & KEASLING, A. 2010. Geochemistry and geochronology of HP mélanges from Tinos and Andros, cycladic blueschist belt, Greece. *Lithos* **117**, 61–81.

BURG, J.-P. 2012. Rhodope: From Mesozoic convergence to Cenozoic extension. Review of petro-structural data in the geochronological frame. *Journal of the Virtual Explorer* **42**, 1–44.

DE CAPITANI, C. & PETRAKAKIS, K. 2010. The computation of equilibrium assemblage diagrams with Theriak/Domino software. *American Mineralogist* **95**, 1006–16.

DI VINCENZO, G., GHIRIBELLI, B., GIORGETTI, G. & PALMERI, R. 2001. Evidence of a close link between petrology and isotop records: constraints from SEM, EMP, TEM and in situ ^{40}Ar-^{39}Ar laser analyses on multiple generations of white micas (Lanterman Range, Antartica). *Earth and Planetary Science Letters* **192**, 389–405.

ERNST, W. G. 1988. Tectonic history of subduction zones inferred from retrograde blueschist P-T paths. *Geology* **16**, 1081–4.

ERNST, W. G. 2001. Subduction, ultrahigh-pressure metamorphism, and regurgitation of buoyant crustal slices: implications for arcs and continental growth. *Physics of the Earth and Planetary Interiors* **127**, 253–75.

EVANS, B. W. 1990. Phase relations in epidote-blueschists. *Lithos* **25**, 3–23.

EVANS, B. W. & BROWN, E. H. (eds) 1986. *Blueschists and Eclogites*. Geological Society of America, Memoir no. 164.

FAUPL, P., PAVLOPOULOS, A. & MIGIROS, G. 1999. The Palaeogene history of the Pelagonian Zone sl (Hellenides, Greece). Heavy mineral study from terrigenous flysch sediments. *Geologica Carpathica* **50**, 449–58.

FAUPL, P., PETRAKAKIS, K., MIGIROS, G. & PAVLOPOULOS, A. 2002. Detrital blue amphiboles from the western Othrys Mountain and their relationship to the blueschist terrains of the Hellenides (Greece). *International Journal of Earth Sciences* **91**, 433–44.

GAUTIER, P., BRUN, J. P. & JOLIVET, L. 1993. Structure and kinematics of Upper Cenozoic extensional detachment on Naxos and Paros (Cyclades Islands, Greece). *Tectonics* **12**, 1180–94.

GRASEMANN, B., SCHNEIDER, D. A., STÖCKLI, D. & IGLSEDER, C. 2012. Miocene bivergent crustal extension in the Cyclades (Greece). *Lithosphere* **4**, 23–39.

HARRISON, T. M., CÉLÉRIER, J., AIKMAN, A. B., HERMANN, J. & HEIZLER, M. T. 2009. Diffusion of ^{40}Ar in muscovite. *Geochimica Cosmochimica Acta* **73**, 1039–51.

HOLLAND, T. J. B. & POWELL, R. 1998. An internally consistent thermodynamic data set for phases of petrological interest. *Journal of Metamorphic Geology* **16**, 309–43.

HUET, B., LABROUSSE, L. & JOLIVET, L. 2009. Thrust or detachment? Exhumation processes in the Aegean: insight from a field study on Ios (Cyclades, Greece). *Tectonics* **28**, doi: 10.1029/2008TC002397.

HUET, B., LE POURHIET, L., LABROUSSE, L., BUROV, E. & JOLIVET, L. 2011*a*. Formation of metamorphic core complex in inherited wedges: a thermomechanical modeling study. *Earth and Planetary Science Letters* **309**, 249–57.

HUET, B., LE POURHIET, L., LABROUSSE, L., BUROV, E. & JOLIVET, L. 2011*b*. Post-orogenic extension and metamorphic core complexes in a heterogeneous crust; the role of crustal layering inherited from collision. Application to the Cyclades (Aegean domain). *Geophysical Journal International* **184**(2), 611–25, doi: 10.1111/j.1365-246X.2010.04849.x.

HUYSKENS, M. H. & BRÖCKER, M. 2014. The status of the Makrotantalon Unit (Andros, Greece) within the structural framework of the Attic-Cycladic Crystalline Belt. *Geological Magazine* **151**(3), 430–46, doi: 10.1017/S0016756813000307.

JACOBSHAGEN, V. 1986. *Geologie von Griechenland*. Berlin: Gebruder Borntraeger.

JACOBSHAGEN, V., DÜRR, S., KOCKEL, F., KOPP, K. O., KOWALCZYK, G., BERCKHEMER, H. & BÜTTNER, D. 1978. Structure and geodynamic evolution of the Aegean region. In *Alps, Apennines, Hellenides* (eds H. Cloos, D. Roeder & K. Schmidt), pp. 537–64. Stuttgart: IUGG.

JOLIVET, L. & BRUN, J. P. 2010. Cenozoic geodynamic evolution of the Aegean. *International Journal of Earth Sciences* **99**, 109–38, doi: 10.1007/s00531-008-0366-4.

JOLIVET, L. & FACCENNA, C. 2000. Mediterranean extension and the Africa-Eurasia collision. *Tectonics* **19**, 1095–106.

JOLIVET, L., FACCENNA, C., HUET, B., LABROUSSE, L., LE POURHIET, L., LACOMBE, O., LECOMTE, E., BUROV, E., DENÈLE, Y., BRUN, J.-P., PHILIPPON, M., PAUL, A., SALAÜN, G., KARABULUT, H., PIROMALLO, C., MONIÉ, P., GUEYDAN, F., OKAY, A., OBERHÄNSLI, R., POURTEAU, A., AUGIER, R., GADENNE, L. & DRIUSSI, O. 2012. Aegean tectonics: Strain localisation, slab tearing and trench retreat. *Tectonophysics* **597–598**, 1–33.

JOLIVET, L., LECOMTE, E., HUET, B., DENELE, Y., LACOMBE, O., LABROUSSE, L., LE POURHIET, L. & MEHL, C. 2010. The North Cycladic detachment system. *Earth and Planetary Science Letters* **289**, 87–104.

JOLIVET, L. & PATRIAT, M. 1999. Ductile extension and the formation of the Aegean Sea. In *The Mediterranean Basins: Tertiary Extension within the Alpine Orogen* (eds B. Durand, L. Jolivet, F. Horvàth & M. Séranne), pp. 427–56. Geological Society of London, Special Publication no. 156.

JOLIVET, L., RIMMELÉ, G., OBERHÄNSLI, R., GOFFÉ, B. & CANDAN, O. 2004. Correlation of syn-orogenic tectonic and metamorphic events in the Cyclades, the Lycian Nappes and the Menderes massif, geodynamic implications. *Bulletin de la Société Géologique de France* **175**(3), 217–38.

KATZIR, Y., AVIGAD, D., MATTHEWS, A., GARFUNKEL, Z. & EVANS, B. 2000. Origin, HP/LT metamorphism and cooling of ophiolitic mélanges in southern Evia (NW Cyclades), Greece. *Journal of Metamorphic Geology* **18**, 699–718.

LACASSIN, R., ARNAUD, N., LELOUP, P. H., ARMIJO, R. & MEYER, B. 2007. Syn- and post-orogenic exhumation of metamorphic rocks in North Aegean. *eEarth* **2**, 51–63.

LAGOS, M., SCHERER, E. E., TOMASCHEK, F., MÜNKER, C., KEITER, M., BERNDT, J. & BALLHAUS, C. 2007. High precision Lu/Hf geochronology of Eocene eclogite-facies rocks from Syros, Cyclades, Greece. *Chemical Geology* **243**, 16–35.

LEAKE, B. E., WOOLLEY, A. R., BIRCH, W. D., BURKE, E. A. J., FERRARIS, G., GRICE, J. D., HAWTHORNE, F. C., KISCH, H. J., KRIVOVICHEV, V. G., SCHUMACHER, J. C., STEPHENSON, N. C. N. & WHITTAKER, E. J. W. 2007. Nomenclature of amphiboles: Additions and revisions to the International Mineralogical Association's amphibole nomenclature. *American Mineralogist* **89**, 883–7.

LECOMTE, E., JOLIVET, L., LACOMBE, O., DENÈLE, Y., LABROUSSE, L. & LE POURHIET, L. 2010. Geometry and kinematics of Mykonos detachment, Cyclades, Greece: evidence for slip at shallow dip. *Tectonics* **29**(5), doi: 10.1029/2009TC002564.

LE PICHON, X. & ANGELIER, J. 1981. The Aegean Sea. *Philosophical Transactions of the Royal Society of London* **300**, 357–72.

LIPS, A. L. W., WHITE, S. H. & WIJBRANS, J. R. 1998. ^{40}Ar/^{39}Ar laserprobe direct dating of discrete deformational events: a continuous record of early Alpine tectonics in the Pelagonian Zone, NW Aegean area, Greece. *Tectonophysics* **298**, 133–53.

LIPS, A. L. W., WIJBRANS, J. R. & WHITE, S. H. 1999. New insights from ^{40}Ar/^{39}Ar laserprobe dating of white mica fabrics from the Pelion Massif, Pelagonian Zone, Internal Hellenides, Greece: implications for the timing of metamorphic episodes and tectonic events in the Aegean region. In *The Mediterranean Basins: Tertiary Extension within the Alpine Orogen* (eds B. Durand, L. Jolivet, F. Horvàth & M. Séranne), pp. 456–74. Geological Society of London, Special Publication no. 156.

LISTER, G. S. & BALDWIN, S. L. 1996. Modelling the effect of arbitrary P-T-t histories on argon diffusion in minerals using the MacArgon program for the Apple MacIntosh. *Tectonophysics* **253**, 83–110.

MALUSKI, H., VERGELY, P., BAVAY, D., BAVAY, P. & KATSIKATSOS, G. 1981. ^{40}Ar/^{39}Ar dating of glaucophanes and phengites in southern Euboa (Greece), geodynamic implications. *Bulletin de la Société Géologique de France* **5**, 469–76.

MASSONNE, H. J. & SCHREYER, W. 1987. Phengite geobarometry based on the limiting assemblage with K-feldspar, phlogopite and quartz. *Contributions to Mineralogy and Petrology* **96**, 212–24.

MAUREL, O., MONIÉ, P., RESPAUT, P., LEYRELOUP, A. F. & MALUSKI, H. 2003. Pre-metamorphic ^{40}Ar/^{39}Ar and U-Pb ages in HP metagranitoids from the Hercynian belt (France). *Chemical Geology* **193**, 195–214.

MEHL, C., JOLIVET, L., LACOMBE, O., LABROUSSE, L. & RIMMELE, G. 2007. Structural evolution of Andros (Cyclades, Greece): a key to the behaviour of a (flat) detachment within an extending continental crust. In *The geodynamics of the Aegean and Anatolia* (eds T. Taymaz, Y. Yilmaz & Y. Dilek), pp. 41–73. Geological Society of London, Special Publication no. 291.

MEYRE, C., DE CAPITANI, C., ZACK, T. & FREY, M. 1999. Petrology of high-pressure metapelites from the Adula Nappe (Central Alps, Switzerland). *Journal of Petrology* **40**, 199–213.

MONIÉ, P. & AGARD, P. 2009. Coeval blueschist exhumation along thousands of kilometers: implications for subduction channel processes. *Geochemistry Geophysics Geosystems* **10**(7), doi: 10.1029/2009GC002428.

MULCH, A. & COSCA, M. A. 2004. Recrystallization or cooling ages: in situ UV-laser ^{40}Ar/^{39}Ar geochronology of muscovite in mylonitic rocks. *Journal of the Geological Society* **161**, 573–82.

MÜLLER, W. 2003. Strengthening the link between geochronology, textures and petrology. *Earth and Planetary Science Letters* **206**, 237–51.

PAPANIKOLAOU, D. J. 1978. Contribution to the geology of the Aegean Sea: the island of Andros. *Annales Géologiques des Pays Helléniques* **29**, 477–553.

PARRA, T., VIDAL, O. & AGARD, P. 2002. A thermodynamic model for Fe-Mg dioctahedral K-white micas using data from phase equilibrium experiments and natural pelitic assemblages. *Contributions to Mineralogy and Petrology* **143**, 706–32.

PARRA, T., VIDAL, O. & JOLIVET, L. 2002. Relation between deformation and retrogression in blueschist metapelites of Tinos island (Greece) evidenced by chlorite-mica local equilibria. *Lithos* **63**, 41–66.

PATZAK, M., OKRUSCH, M. & KREUZER, H. 1994. The Akrotiri Unit of the island of Tinos, Cyclades, Greece: Witness to a lost terrane of Late Cretaceous age. *Neues Jahrbuch für Geologie und Paläontologie Abhandlungen* **194**, 211–52.

PHILIPPON, M., BRUN, J.-P. & GUEYDAN, F. 2012. Deciphering subduction from exhumation in the segmented Cycladic Blueschist Unit (Central Aegean, Greece). *Tectonophysics* **524–525**, 116–34.

PUTLITZ, B., COSCA, M. A. & SCHUMACHER, J. C. 2005. Prograde mica ^{40}Ar/^{39}Ar growth ages recorded in high pressure rocks (Syros, Cyclades, Greece). *Chemical Geology* **214**, 79–98.

REINECKE, T. 1986. Phase relationships of sursassite and other Mn-silicates in highly oxidized low-grade, high-pressure metamorphic rocks from Evvia and Andros Islands, Greece. *Contributions to Mineralogy and Petrology* **84**, 110–26.

RING, U., GLODNY, J., WILL, T. & THOMSON, S. 2007*a*. An Oligocene extrusion wedge of blueschist-facies nappes on Evia, Aegean Sea, Greece; implications for the early exhumation of high-pressure rocks. *Journal of the Geological Society of London* **164**, 637–52.

RING, U., GLODNY, J., WILL, T. & THOMSON, S. 2010. The Hellenic subduction system: high-pressure metamorphism, exhumation, normal faulting, and large-scale

extension. *Annual Review of Earth and Planetary Sciences* **38**, 45–76.

RING, U., WILL, T., GLODNY, J., KUMERICS, C., GESSNER, K., THOMSON, S., GUNGOR, T., MOIE, P., OKRUSCH, M. & DRUEPPEL, K. 2007*b*. Early exhumation of high pressure rocks in extrusion wedges; Cycladic blueschist unit in the eastern Aegean, Greece, and Turkey. *Tectonics* **26**(2), doi: 10.1029/2005TC001872.

SCHERMER, E. R. 1990. Mechanism of blueschist creation and preservation in a A-type subduction zone, Mount Olympos region, Greece. *Geology* **18**, 1130–3.

SCHERMER, E. R., LUX, D. R. & BURCHFIEL, B. C. 1990. Temperature-time history of subducted continental crust, Mount Olympos region, Greece. *Tectonics* **9**, 1165–95.

SCHLIESTEDT, M. 1986. Eclogite-blueschist relationships as evidenced by mineral equilibria in the high-pressure metabasic rocks of Sifnos (Cycladic Islands). *Journal of Petrology* **27**, 1437–59.

SCHNEIDER, J., BOSCH, D., MONIÉ, P. & BRUGUIER, O. 2007. Micro-scale element migration during eclogitisation in the Bergen arcs (Norway): a case study on the role of fluids and deformation. *Lithos* **96**(3), 325–52.

THOMPSON, A. B. & ENGLAND, P. C. 1984. Pressure-temperature-time paths of regional metamorphism II. Their inference and interpretation using mineral assemblages in metamorphic rocks. *Journal of Petrology* **25**, 929–55.

TOMASCHEK, T., KENNEDY, A. K., VILLA, I. M., LAGOS, M. & BALLHAUS, C. 2003. Zircons from Syros, Cyclades, Greece: Recrystallization and mobilization of zircon during high-pressure metamorphism. *Journal of Petrology* **44**, 1977–2002.

TROTET, F., JOLIVET, L. & VIDAL, O. 2001. Tectono-metamorphic evolution of Syros and Sifnos islands (Cyclades, Greece). *Tectonophysics* **338**, 179–206.

TROTET, F., VIDAL, O. & JOLIVET, L. 2001. Exhumation of Syros and Sifnos metamorphic rocks (Cyclades, Greece). New constraints on the P-T paths. *European Journal of Mineralogy* **13**, 901–20.

VIDAL, O., DE ANDRADE, V., LEWIN, E., MUNOZ, M., PARRA, T. & PASCARELLI, S. 2006. P-T-deformation-Fe^{3+}/Fe^{2+} mapping at the thin section scale and comparison with XANES mapping: application to a garnet-bearing meta-pelite from the Sambagawa metamorphic belt (Japan). *Journal of Metamorphic Geology* **24**, 669–83.

VIDAL, O. & PARRA, T. 2000. Exhumation paths of high pressure metapelites obtained from equilibria for chlorite-phengite assemblages. *Geological Journal* **35**, 139–61.

VIDAL, O., PARRA, T. & TROTET, F. 2001. A thermodynamic model for Fe-Mg aluminous chlorite using data from phase equilibrium experiments and natural pelitic assemblages in the 100–600 °C, 1–25 kbar range. *American Journal of Science* **6**, 557–92.

VILLA, I. M. 1998. Isotopic closure. *Terra Nova* **10**, 42–7.

VILLA, I. M. & WILLIAMS, M. L. 2012. Geochronology of metasomatic events. In *Metasomatism and the Chemical Transformation of Rock* (eds D. E. Harlov & H. Austrheim), pp. 171–202. Berlin: Springer-Verlag.

WARREN, C. J., HANKE, F. & KELLEY, S. P. 2012. When can muscovite $^{40}Ar/^{39}Ar$ dating constrain the timing of metamorphic exhumation? *Chemical Geology* **291**, 79–86.

WHITNEY, D. L. & EVANS, B. W. 2010. Abbreviations for names of rock-forming minerals. *American Mineralogist* **95**, 185–7.

WIJBRANS, J. R. & MCDOUGALL, I. 1986. $^{40}Ar/^{39}Ar$ dating of white micas from an alpine high-pressure metamorphic belt on Naxos (Greece); the resetting of the argon isotopic system. *Contributions to Mineralogy and Petrology* **93**, 187–94.

WIJBRANS, J. R. & MCDOUGALL, I. 1988. Metamorphic evolution of the Attic Cycladic Metamorphic Belt on Naxos (Cyclades, Greece) utilizing $^{40}Ar/^{39}Ar$ age spectrum measurements. *Journal of Metamorphic Geology* **6**, 571–94.

YAMATO, P., AGARD, P., GOFFÉ, B., DE ANDRADE, V., VIDAL, O. & JOLIVET, L. 2007. New, high-precision P–T estimates for Oman blueschists: implications for obduction, nappe stacking and exhumation processes. *Journal of Metamorphic Geology* **25**, 657–82.

ZEFFREN, S., AVIGAD, D., HEIMANN, A. & GVIRTZMAN, Z. 2005. Age resetting of hanging wall rocks above a Tertiary low-angle detachment, Tinos island, Aegean Sea. *Tectonophysics* **400**, 1–25.

ZIV, A., KATZIR, Y., AVIGAD, D. & GARFUNKEL, Z. 2010. Strain development and kinematic significance of the Alpine folding on Andros (western Cyclades, Greece). *Tectonophysics* **488**, 248–55.